Hindawi
Geofluids
Volume 2023, Article ID 8859177, 22 pages
https://doi.org/10.1155/2023/8859177

Research Article

Fracture Initiation and Propagation in the Hot Dry Rock Subject to the Cyclic Injection Hydraulic Fracturing Treatment

Yilong Yuan,[1,2] **Wei Wang**,[2,3] **Jiawei Tang**,[1] **Qiang Guo**,[1] **and Yulong Liu**[2,4]

[1]*State Key Laboratory of Water Resource Protection and Utilization in Coal Mining, Beijing 102209, China*
[2]*Key Laboratory of Groundwater Resources and Environment, Ministry of Education, Jilin University, Changchun 130021, China*
[3]*Sichuan Institute of Geological Engineering Investigation Group Co. Ltd., Chengdu 610072, China*
[4]*School of Petroleum Engineering, Yangtze University, National Engineering Research Center for Oil & Gas Drilling and Completion Technology, Wuhan 430100, China*

Correspondence should be addressed to Yulong Liu; yulongliu@jlu.edu.cn

Received 16 May 2023; Revised 16 September 2023; Accepted 9 October 2023; Published 16 November 2023

Academic Editor: Shuyang Liu

Cyclic injection hydraulic fracturing is a promising way for the geothermal energy exploitation by reactivating the fractures in geothermal reservoir. However, fracture initiation and growth induced by cyclic injection schemes have been inadequately studied for hot dry rock (HDR), and the cyclic injection fracturing optimized often by experience. For this reason, the initiation and propagation of hydraulic fractures in the HDR under different cyclic injection methods were determined by experiment research for hydraulic fracturing. The results show that the cyclic frequency and injection rate play different roles in the stimulation of HDR. The cyclic injection with low frequency-low pressure can create more branched fractures, forming a short but complex hydraulic fracture network. However, when high flow-high frequency injection method is subjected, the branch fractures formed are significantly reduced, but each branch fracture can be fully expanded. To fully exploit the advantages of different injection methods, a numerical model that contains a fracture network was established with PFC software, and an alternating cyclic injection scheme with synergistic control of the cyclic frequency and injection rate was proposed. The comparison results indicated that the alternating cyclic injection method can effectively improve the fracturing effect in the HDR. The stimulation area of the alternating cyclic injection method is about 2.3 times and 2.7 times that of the low flow-low frequency and high flow-high frequency injection methods, respectively. The method presented here can be adopted to optimize the fracture growth regime and provide a scientific basis for EGS hydraulic fracturing design.

1. Introduction

Hot dry rock (HDR) is a high-temperature rock without water (or with a small amount of water but not flowing), which can be artificially fractured to form an enhanced geothermal system (EGS) to extract a large amount of thermal energy from deep underground. At present, HDR is a clean energy with the most application value and potential in the 21st century as its advantages of cleanness, wide distribution, and large resource reserves [1, 2].

Hydraulic shear, which aims to shear more preexisting fractures, has become the key technology widely used in the stimulation of HDR reservoirs [3, 4]. However, so far, this design has achieved only limited success. Studies have shown that short circuits or severe reservoir leakage still occurs even the fracture-developed zones in EGS were directionally fractured [5–7]. This is because, only by injecting water into a single open-hole section, the fluid flow tends to be localized in a few main flow paths, and the natural fractures in HDR are difficult to be sheared and activated [8]. Without substantial flow paths, thermal storage lacks the ability to maintain high-velocity flow, resulting in poor fracturing effect of the reservoir [9–11]. Additionally, hydraulic stimulation aimed at creating commercial reservoirs may generate seismic events, resulting in a negative public perception of EGS. For example, the seismic event ($M = 3.4$) triggered by the hydraulic stimulation of Basel in Switzerland has led to the (preliminary) termination of the project

[3]. In the Soultz in France and Cooper in Australia, hydraulic fracturing also induced a series of seismic events, with the highest magnitudes reaching $M = 2.9$ and $M = 3.7$, respectively. Therefore, the main challenge for the effective development of HDR is to construct a more complex fracture network under the premise of safe stimulation measures, to achieve the best heat transfer performance of the enhanced geothermal system (EGS) [12–14].

Cyclic injection is a promising solution for the HDR hydraulic fracturing [15–17]. Experiments performed by Zang et al. [18] have proved that the monotonic increase in load with time can produce a wider fracture process zone. However, the constant loading interrupted by cycles of alternating high and low injection rate has no further deformation, which leads to narrow areas of tensile and shear fractures [19, 20]. By contrast, laboratory experiments conducted by [21] determined that the cyclic injection has obvious advantages in reducing the fracturing pressure of Pocheon granite. Frequent starting and stopping of loading causes fatigue fracture of the rock, and the area of cyclic injection, that is, the stimulated volume, is larger than that of monotonic injection. Additionally, the number of events, as well as their magnitudes, was found to be lower compared to those during continuous injection [13, 22, 23]. The reason is that mechanical fatigue is highly dependent on the frequency of loading and the type of material. The propagation of microcracks caused by fatigue during cyclic injection can be envisioned to involve more fluid-rock interactions, thus resulting the larger stimulated area and the lower seismic magnitude generation [24–26].

Cyclic injection is expected to be an alternative to the HDR hydraulic fracturing treatment [27, 28]. However, the hydraulic fracturing scheme using cyclic injection is still in the proof-of-concept stage, and the initiation and propagation mechanism of hydraulic fractures in HDR under different cyclic injection methods is inadequately studied [15, 29, 30]. Lacking of theoretical guidance, the hydraulic fracturing of HDR based on the cyclic injection does not reduce the risk of large earthquakes; the effect of reservoir permeability enhancement is also unsatisfactory [31, 32]. Predictably, the key cyclic hydraulic fracturing parameters (injection rate and cycle frequency) play different roles in the stimulation of HDR, and different combinations of the two (different cyclic injection methods) may have a significant impact on the initiation and propagation of hydraulic fractures in HDR. Therefore, it is necessary to systematically study the initiation and propagation of hydraulic fractures under different cyclic injection methods.

At present, the researches on hydraulic fracturing of HDR almost focus on hydraulic fracturing under a single cyclic injection method. To our knowledge, few publications have been published so far on when alternative cyclic injection methods were adopted. Therefore, a true triaxial hydraulic fracturing system was adapted to systematically study the initiation and propagation of hydraulic fractures in HDR under different cyclic injection methods. On this basis, by constructing a discrete fracture network model, the initiation and propagation of hydraulic fractures under single and alternate cyclic injection schemes were determined. As a result, an alternating cyclic injection scheme with synergistic control of the cyclic frequency and injection rate was proposed. The results presented in this work are of great significance for the construction of fracture network and the promotion of large-scale exploitation of geothermal resources from the HDR.

2. Methods

2.1. Physical Experiments

2.1.1. Sample Preparation. The rock samples used in the experiment were taken from the Gonghe Basin in Qinghai Province. The collected samples are gray white in color, hard in texture, and resistant to weathering (Figure 1). Through mechanical testing, the physical and mechanical properties of granite rock samples were obtained, as shown in Table 1.

The sample used in the experiment is 300 mm × 300 mm × 300 mm granite cube. Before the test, a circular hole with a diameter of 16 mm and a depth of 120 mm was vertically drilled at the center of one side of the granite sample to simulate the wellbore. Simulate the wellbore using a stainless steel pipe with an outer diameter of 14 mm and an inner diameter of 10 mm. The simulated wellbore was cemented using temperature resistant epoxy resin (Figure 1).

2.1.2. Experimental Setup. The hydraulic fracturing system upgraded by Jilin University can currently provide an injection pressure of 80 MPa, and the three-dimensional stress can be provided separately as required. The three-dimensional confining pressure can be loaded up to 30 MPa, and the rated load is 18 kW. The heating device can make the working temperature in the sample chamber range from room temperature to the maximum value of 180°C (Figure 2).

Acoustic emission monitoring system is composed of DS2 acoustic emission instrument, supporting acquisition and storage software system, which can realize high-frequency multichannel synchronous acquisition of acoustic emission characteristics (Figure 3). The acoustic emission calculation system can calculate the signal amplitude, energy, occurrence time, and duration of each AE probe, while monitoring the propagation process and morphology of fractures through three-dimensional positioning of 8 AE probes.

2.1.3. Experimental Procedures. The detailed steps of the experiment are as follows: (1) dye the fracturing fluid, fill it into an intermediate container, connect the pipeline, and check the sealing of the pipeline; (2) place the sample in an oven, heat it to 180°C at a heating rate of 5°C/min, and maintain it for 12 hours; (3) after the temperature inside the pressure vessel returns to the target temperature, open the pressure boosting valve of the true triaxial equipment, and load the triaxial stress to the target value through the control system; (4) start the injection pump and conduct the fracturing experiment with the target displacement, and record the fracturing curve; and (5) stop heating the kettle body, open the equipment evacuation valve, unload the pressure, take out the sample, and label it.

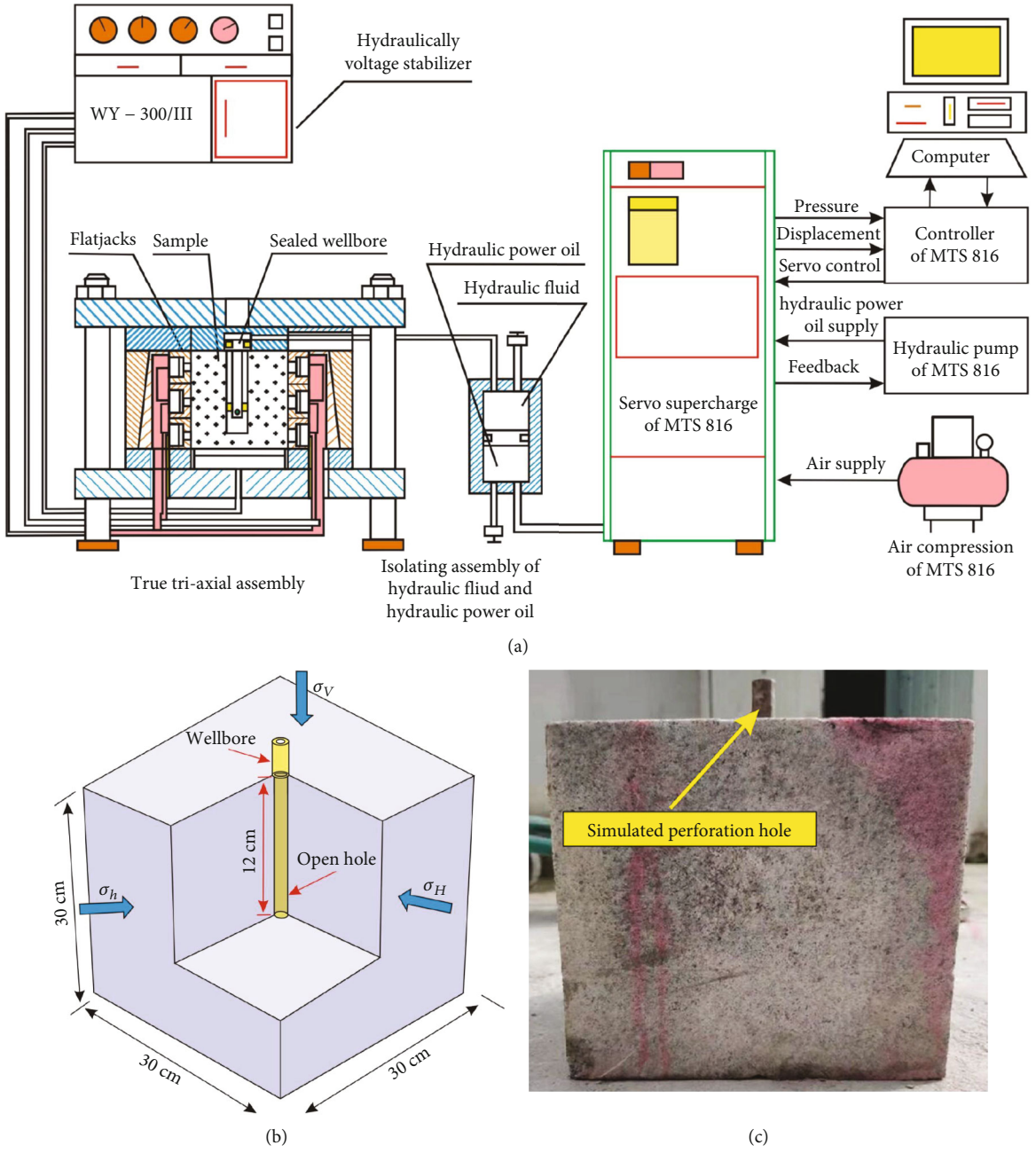

Figure 1: Triaxial hydraulic fracturing platform and sample preparation: (a) triaxial hydraulic fracturing platform; (b) schematic diagram of fracturing sample; (c) prepared rock samples.

Table 1: Basic physical and mechanical properties of the granite samples.

Parameter (unit)	Value
Density (kg/m^3)	2560
Permeability (mD)	0.04
Young's modulus (GPa)	40
Tensile strength (MPa)	19.17
Poisson ratio	0.25
Thermal conductivity (W·m^{-1}·K^{-1})	3.13

After the fracturing is completed, the cubic granite sample is evenly cut into 4 pieces and the expansion morphology of hydraulic fractures inside each piece is observed. Reorganize and reconstruct the observed results of each piece to draw the final expansion morphology of hydraulic fractures in the sample (Figure 4).

2.1.4. Experimental Scheme. The measured vertical principal stress and maximum and minimum horizontal principal stress of the target reservoir in the Gonghe Basin are 50 MPa, 45 MPa, and 35 MPa, respectively. Considering the physical similarity between the fracturing site and the

Figure 2: The true triaxial hydraulic fracturing equipment and test process.

experimental model, the three-dimensional in situ stress in the experiment was set to 20, 18, and 14 MPa, respectively. The temperature of 180° was set in the fracturing test, which is the highest temperature that the system can reach.

To capture the initiation and propagation of hydraulic fractures under different cyclic injection methods, high flow-high cycle interval and low flow-low cycle interval cyclic injection methods were performed on granite specimens A1 and B1, respectively. During cyclic fracturing with the high flow-high cycle interval, the fracturing fluid was injected at the constant rate of 15 mL/min. After maintaining this state for 20 s (cycle interval), the injected fluid decreased to 1 mL/min. For the next 20 s, enter the next cycle (see Figure 5(a)). Compared with high flow-high cycle interval, the cyclic hydraulic fracturing with low flow-low cycle interval increased to 10 mL/min and the cycle interval decreased to 10 s (see Figure 5(b)).

2.2. Discrete Elemental Method. On the basis of laboratory tests, a discrete element fracture network model was constructed by introducing preexisting fractures to analyze the influence of fracture reactivation on the hydraulic fracture initiation and propagation in the HDR.

2.2.1. Fluid-Mechanical Coupling in Particle Flow Program. In the discrete element method (DEM) model, the algorithm of fluid flow is realized based on the subroutine developed by the embedded FISH language. The principle of fluid-mechanical coupling in the DEM model is shown in Figure 6. Two adjacent fluid domains are related through fluid channels and obey the Poiseuille channel flow theory [33]:

$$Q = -\frac{R^3}{12\mu}\frac{(p_2 - p_1)}{l}, \tag{1}$$

where Q is the volume of fluid flowing through the flow channel (cm^3/s), l is the length (cm), R is the pore size of the flow channel (cm), and μ is the fluid viscosity (Pa·s).

According to the fluid-structure coupling relationship of DEM model, the R can be expressed as [34]

$$R = \frac{R_0\sigma_0^n}{\sigma^n + \sigma_0^n}, \tag{2}$$

where R is the pore radius under normal stress (cm), R_0 is the pore radius of the reservoir when no stress is applied (cm), and σ^n and σ_0^n are the normal stress acting on the stratum and pores (MPa).

2.2.2. Model Setup. PFC2D software was used to build the DEM model. The size of the model is 120 × 100 mm. To capture the effect of cyclic injection methods on the propagation of natural fractures, two natural fracture models were set up with a length of 50 mm on both sides of the injection hole (Figure 7(a)). On this basis, multiple natural fractures were preset in the DEM model to further analyze the impact of fracture reactivation on the formation of hydraulic fracture networks in HDR.

In the DEM model, two injection methods as the experimental test were considered: low flow-low frequency and high flow-high frequency cyclic injection methods. The interval of each cycle in the low flow-low cycle interval cyclic injection was 10 s, and the injection rate was set as 1.0 m^2/s. The model cycled 360 times in 120 minutes, and the injection volume is 360 m^2. The interval of each cycle in the high flow-high cycle interval cyclic injection was 20 s, and the injection speed was 2.0 m^2/s. The model cycled 360 times in 240 minutes, and the total injected volume was consistent with the low flow-low cycle interval scheme (i.e., 360 m^2).

In addition, to capture the initiation and propagation of hydraulic fractures under different cyclic injection methods, the in situ stress and injection fluid parameter set in the model are based on the actual data published based on the Gonghe Basin EGS fracturing site [36, 37].

2.3. Model Calibration. To verify the correctness of the DEM model, the triaxial compression tests using the typical granite samples from the Gonghe Basin were conducted, and the accuracy of the model was calibrated. Before the hydraulic fracturing experiment, the remaining rock samples for hydraulic fracturing were cut to a cylindrical sample with the size of 50 × 100 mm. In order to ensure the comparability between the model and the experiment, the stress, temperature, and loading method of the model were consistent with the experiment. The detailed model parameters are summarized in Table 2.

The comparisons with experimental data and numerical simulation data are shown in Figure 8. The comparison results show that the model calculated results are generally in good agreement with the experiment observation. The error between the numerical model and the experiment observation is within an acceptable range.

Based on data fitting, the fracture morphology of the experimental and numerical model was further compared as shown in Figure 9. The comparisons between the

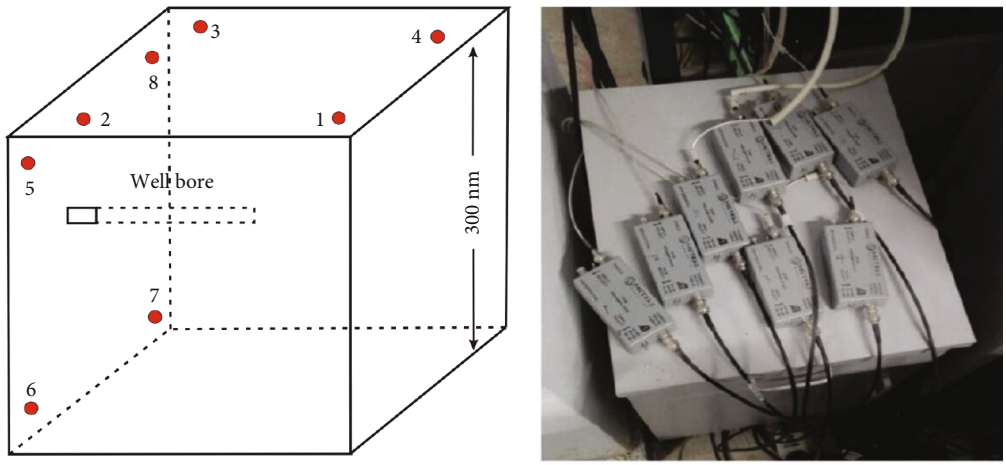

Figure 3: Spatial distribution of acoustic emission probes (a) and acoustic emission sensors (b).

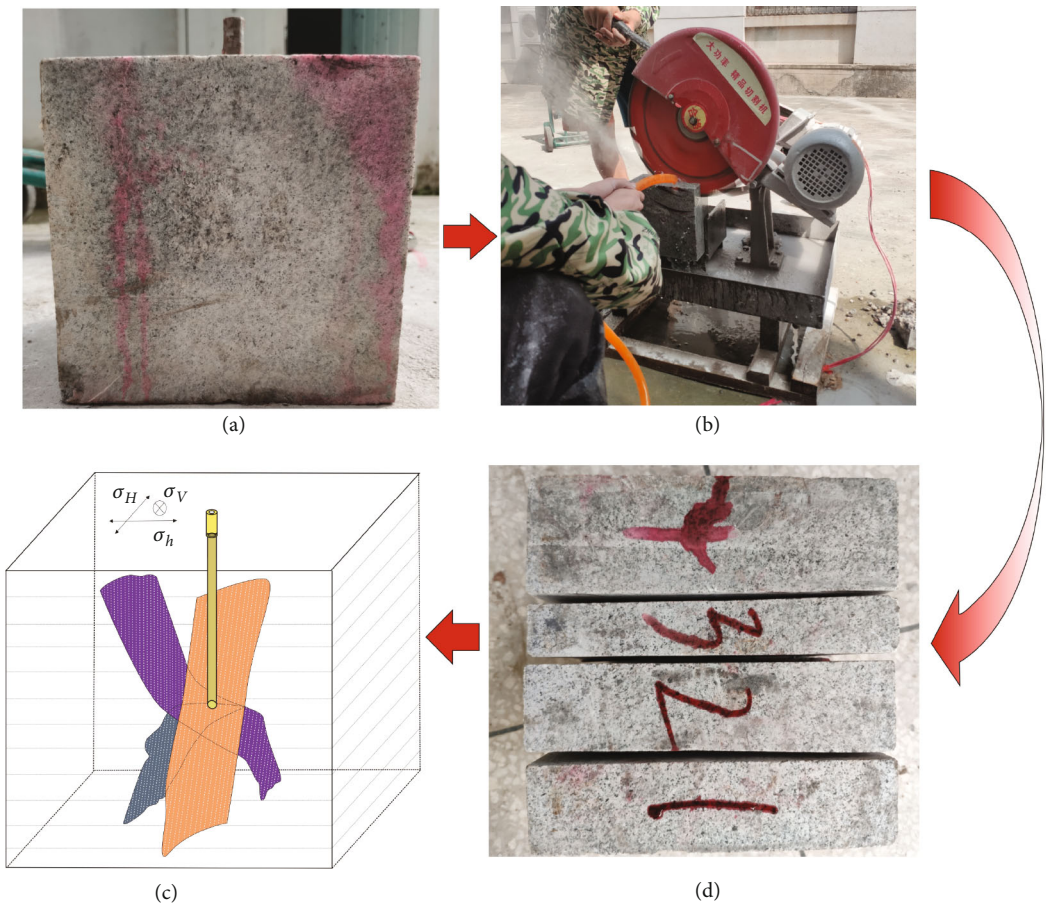

Figure 4: Flow chart of sample cutting and crack description after compaction.

experimental and model simulation showed that the macroscopic fracture morphology of rock has a good correspondence with the simulation results. By comparing the experimental model with numerical simulation results, the accuracy and reliability of the DEM model have been effectively verified. In addition, the macro- and micromodel parameters required by the model have also been further calibrated and given in Table 2.

Based on the triaxial compression experiment, the constitutive model of the numerical procedure was corrected and the macroscopic and microscopic constitutive properties of the HDR were obtained. To comprehensively correct

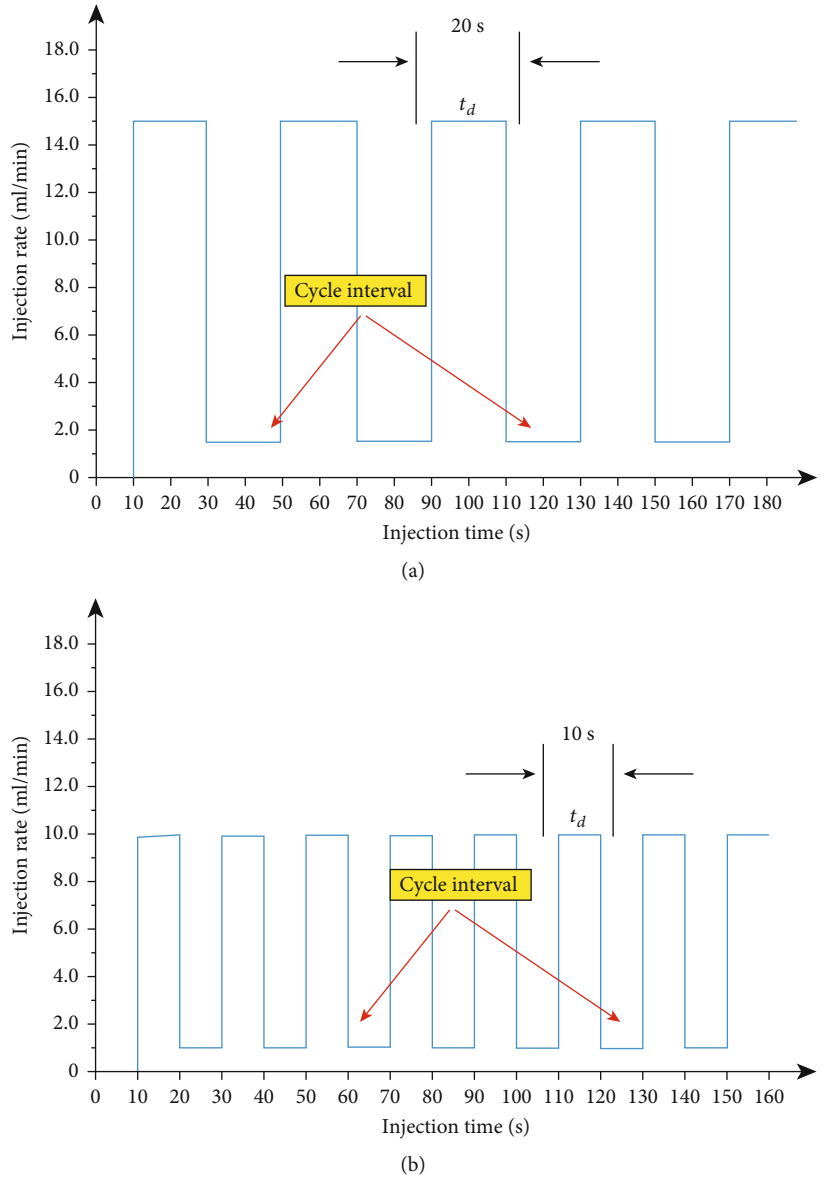

Figure 5: Schematic diagram of different cyclic injection methods: (a) high flow-high cycle interval cyclic injection method; (b) low flow-low cycle interval cyclic injection method.

the accuracy of the model, on the basis of constitutive relationship correction, a large-scale true triaxial hydraulic fracturing test was conducted to further calibrate the fluid-structure coupling of the numerical model.

To make the numerical model comparable with the laboratory experiment, the test conditions (temperature, pressure), rock mechanical parameters, and fluid injection method of the fracturing numerical model are consistent with the experimental model. Figure 10 reflects the hydraulic fracture morphology of the numerical and experimental models. The calibration results show that the hydraulic fracturing forms a main hydraulic fracture and a branch fracture in the direction of maximum principal stress. The morphology of hydraulic fractures formed by experimental and numerical models has high comparability, which perfectly verifies the correctness of the numerical model.

Additionally, the hydraulic fracturing pressure curve of the numerical and experimental models shows that the hydraulic fracturing pressure curve obtained by the numerical model is in good agreement with the experimental model, and there are differences only at the highest and lowest points of the injection pressure curve (Figure 11). This is because real granite samples are not perfectly homogeneous and isotropic; the initiation and propagation of hydraulic fracture can never exactly match the theoretical prediction and numerical modeling. Although there are some differences only at the highest and lowest points of the injection pressure curve, the error maintains at a small value, which verifies the accuracy of the numerical model for simulating the initiation and propagation of hydraulic fractures.

2.4. Model Parameters for Natural Fracture. The criterion proposed by Gu and Weng [38] regarding the nonorthogonal

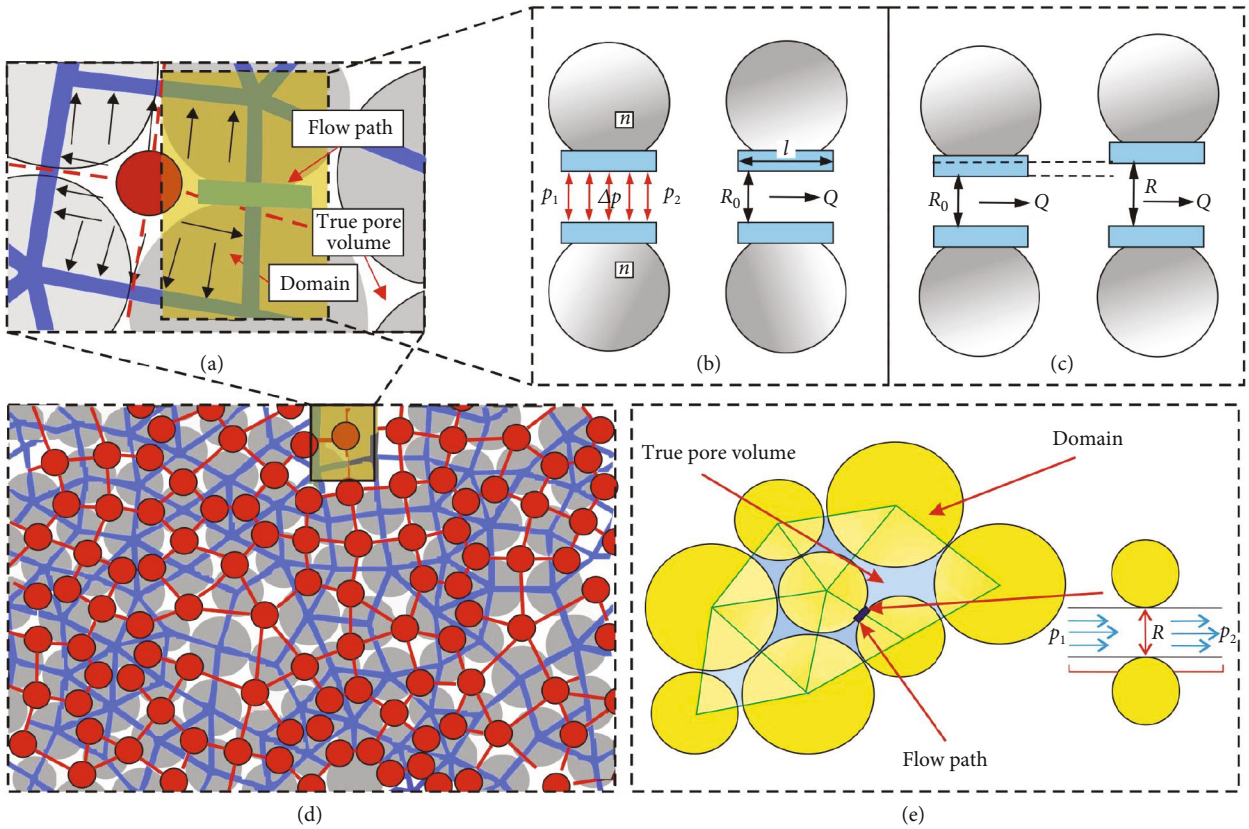

Figure 6: Fluid-structure coupling relationship of DEM model [35].

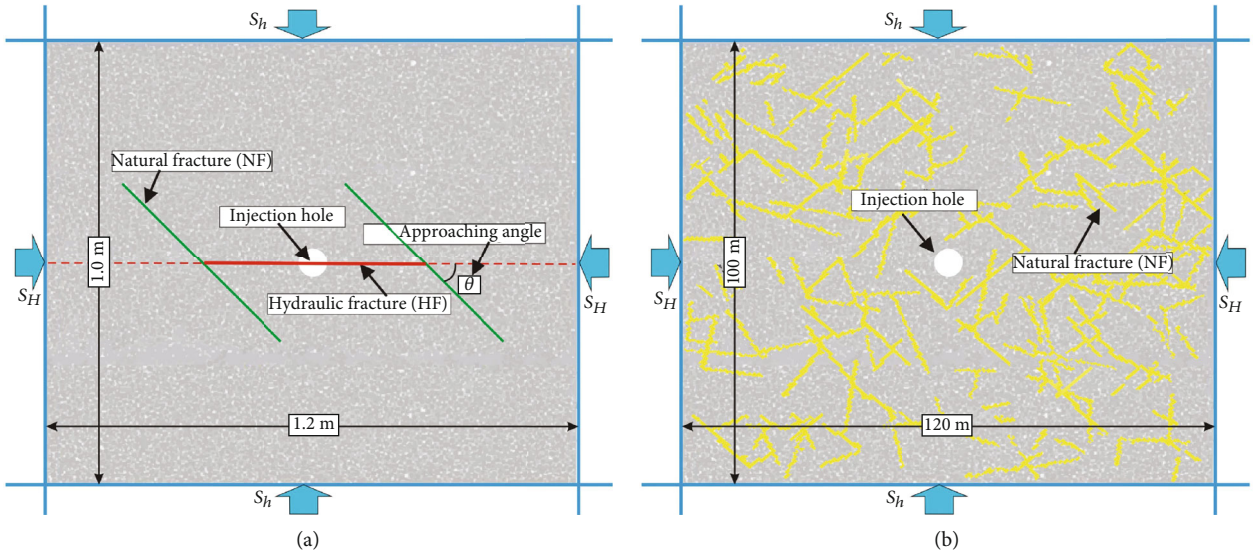

Figure 7: Construction of discrete element model: (a) prefabricated two natural fissures; (b) contains a natural fracture network.

angle of friction interfaces with cohesion indicates that the accuracy of NF parameters is determined by the propagation of hydraulic fracture after the intersection of hydraulic fractures and natural fractures [39]. The critical determination curve of hydraulic fracture crossing natural fractures based on the theoretical criteria proposed by Gu and Weng [38] is shown in Figure 12.

To ensure the accuracy of numerical simulation, nature fracture parameters such as cohesion, friction coefficient, shear stiffness, and tensile strength were selected to be as similar as possible to the actual situation of the reservoir under different stress ratios, friction coefficients, and approach angle [40]. Therefore, the nonorthogonal angle criterion of natural fracture friction interface proposed by

Table 2: The macroscopic and microscopic parameters of the model after experimental calibration.

Category	Parameters	Value
Bonded particle	Density (kg/m^3)	2600
	Particle radius R_{min} (mm)	0.25
	Radius ratio R_{max}/R_{min}	1
	Young's modulus (GPa)	62
	Normal and tangential stiffness ratio k_n/k_s	1.7
	Friction coefficient	0.5
Contact characteristics	Cohesion (MPa)	30
	Tensile strength (MPa)	9
	Angle of internal friction (°)	52

Gu and Weng was adopted, and the relevant parameters of natural fractures in the model were calibrated.

Figure 13 shows the comparison of the hydraulic fractures and natural fracture interaction results under different conditions. In most cases, there is good consistency between numerical simulation and theoretical analysis. Based on the validation between theoretical model and numerical simulation, the properties of natural fractures in the model were corrected and the parameters of natural fractures in the model were obtained (Table 3).

3. Results and Analyses

3.1. Hydraulic Fracturing Experiment of HDR under Different Cyclic Injection Methods

3.1.1. The Cyclic Injection with High Flow-High Cycle Interval

(1) AE Characteristics during Hydraulic Fracturing. Combining the pressure data with the acoustic emission to analyze the activity and concentration of the acoustic emission source can comprehensively understand the fracture initiation and propagation during hydraulic fracturing of the HDR [41]. The injection pressure and acoustic emission energy level of sample A1 are shown in Figure 14. The results show that the curve of injection pressure under the cyclic injection with high flow-high cycle interval can be divided into three stages.

Stage I is the prefracturing stage, in which the fracturing fluid fills the wellbore and the pressure rises to 15.4 MPa. The second stage is the crack initiation stage of the granite specimen. As the fracturing fluid is injected into the granite specimen, the injection pressure rises to the breakdown pressure point (Figure 14). At the breakdown pressure point, the injection pressure reaches a peak pressure of 34.45 MPa, the fracture curve drops sharply, and the pressure drop can reach 16 MPa (Figure 14). A higher pressure drop indicates that the rock releases higher energy during fracture, and the macrofracture extension ability is stronger. In stage III, the injection pressure gradually decreased and the frequency of acoustic emission activities was very low. This further proved that fracturing opening occurred in the second stage.

(2) Hydraulic Fracture Morphology. The location points of acoustic emission can reflect the gradual damage of the material and then reveal the evolution process of fractures in the granite specimen [42]. Figure 15 shows the spatial distribution of acoustic emission points under the cyclic injection with high flow-high cycle interval.

The results show that from the acoustic emission localization of the whole test, the localization points are mainly concentrated in the center of the wellbore and distributed in a band along the path of the fracture surface, and the overall number of acoustic emission events is small (Figure 15(d)). Figure 11 shows the fracture morphology of specimen A1 after fracturing. The results show that the hydraulic fracture mainly extends along the maximum principal stress (MPS) and penetrates the front and bottom surfaces of the specimen. In addition, a branch fracture was formed in the direction with an angle of 30° to the MPS. The geometry of fractures in Figure 16 corresponds well with the acoustic emission location of the specimen.

The results show that the pulse pressure wave formed by cyclic injection with high flow-high cycle interval is strong and easy to form a single main fracture (defect) in the rock. However, despite the relatively simple morphology of these main cracks, they have a strong ability to extend (advantage).

3.1.2. The Cyclic Injection with Low Flow-Low Cycle Interval

(1) AE Characteristics during Hydraulic Fracturing. Figure 17 shows the pump pressure curve of specimen B1 against the acoustic emission sequence. During the initial stage of prefracturing, the frequency of acoustic emission activities is not high, and only a few low-energy-level acoustic emission events occur. As the injection pressure increases, the fluid pressure fluctuation becomes larger, and the high-energy-level acoustic emission events are distributed in clusters. This indicates that fatigue damage occurs in the rock, and the microcracks of internal defects are aggregated and nucleated with the increase of the number of cycles. After reaching the peak pressure, the fluid pressure fluctuation decreases slowly. At this time, there are still high-energy acoustic emission events distributed in clusters, indicating that the cracks are still forming and expanding.

(2) Hydraulic Fracture Morphology. The spatial distribution of acoustic emission points under the cyclic injection with low flow-low cycle interval is shown in Figure 18. In the early stage, the AE points are only distributed in the center of the sample, and the cracks are in the stage of scattered initiation (Figure 18(a)). With the increase of injection volume, the AE points become dense at the center and spread radially from the center to the surrounding (Figure 18(b)). The further accumulation of fluid pressure makes the AE events evenly generated around the channel path generated in the previous stage, which indicates that a considerable number

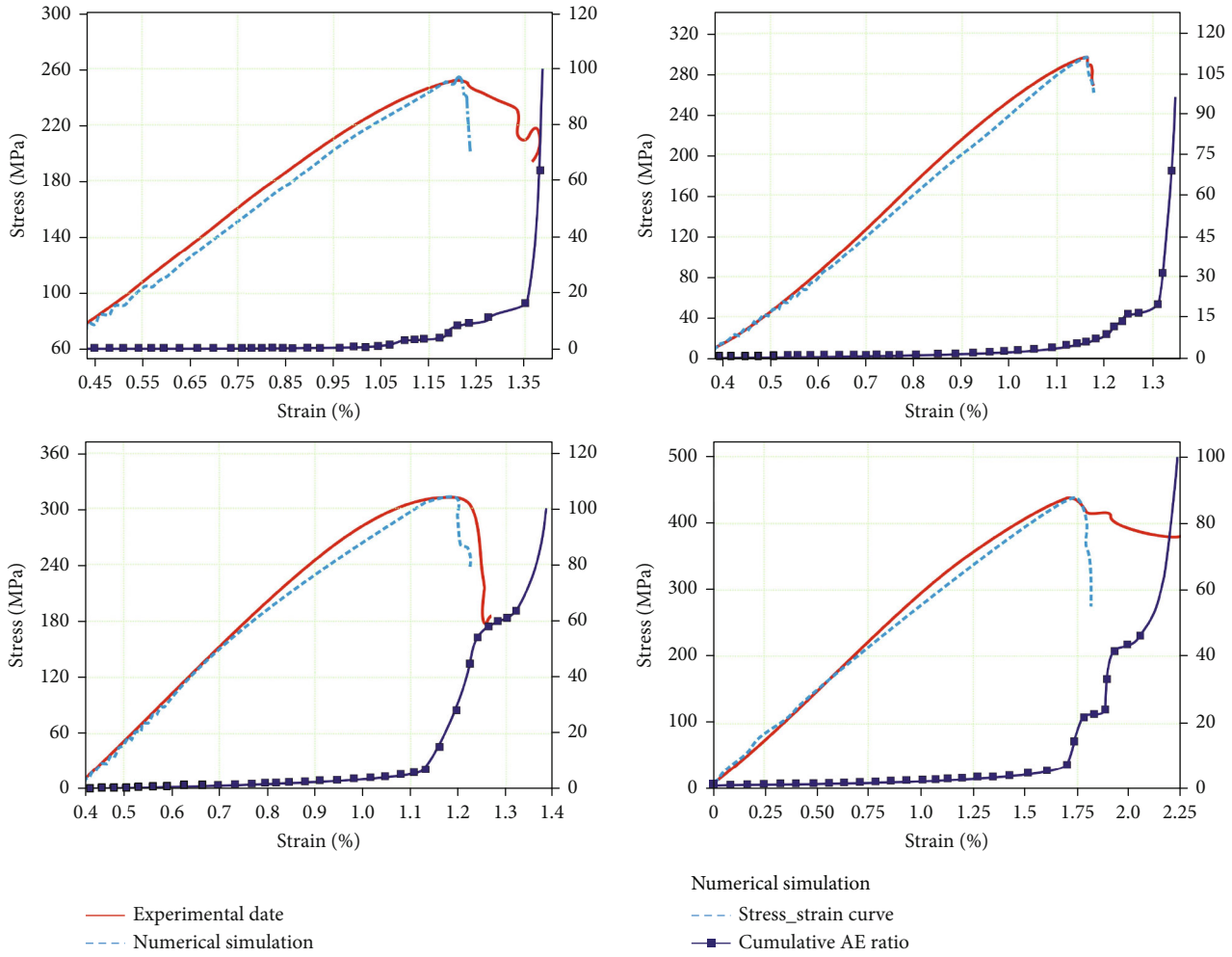

Figure 8: Inversion correction of numerical model and physical compression.

of secondary cracks have been formed in the specimen (Figure 18(c)). After fracturing, the AE events are distributed radially from the injection point to the surrounding (Figure 18(d)). However, the formed fracturing fractures are limited to the surrounding of the wellbore, far from reaching the surface of the specimen.

In addition, judging from the actual fractures of specimen B1, the cyclic injection with low flow-low cycle interval can form complex radial-shaped fractures. However, due to the low injection pressure, the formed complex fracture network has a limited scope (Figure 19), which is in good agreement with the acoustic emission location of the specimen.

High flow-high cycle interval cyclic injection can easily form fractures with single morphology but strong extensibility; while the fractures formed by low flow-low cycle interval cyclic injection are complex but have a short extension range. However, based on the development concept of the HDR, the hydraulic fracturing technology requires not only the formation of complex propagation paths in the target reservoir but also requires that the fractures can be fully expanded. Therefore, to fully exploit the merits of the different cyclic injection schemes, a combination of the two injection methods was proposed and the hydraulic fracturing experiments were further conducted. In the early stages of hydraulic fracturing, the low flow with low cycle interval cyclic injection method was adapted to generate more branching fractures. After that, the high-pressure injection method (high flow-high cycle interval) was alternately adopted to further expand the branching formed by the early stages, thereby forming a larger fracture network.

The morphology of the hydraulic fracture network under alternating cyclic injection is shown in Figure 20. The experimental results show that compared to a single hydraulic fracture created by high flow-high cycle interval, multiple branch fractures (8 branch fractures) were formed in the HDR under alternating cyclic injection. Compared to the complex with short extension fracture network formed by low flow-low cycle interval, each branch fracture formed by alternating cyclic injection in HDR has been fully expanded.

3.2. Fracture Network Simulation of HDR under Different Cyclic Injection Methods. The experiment preliminarily proves that the cyclic injection method of low flow-low cycle interval + high flow-high cycle interval is beneficial for fully utilizing the advantages of each injection method and forming good fracturing effects in HDR. However, compared to

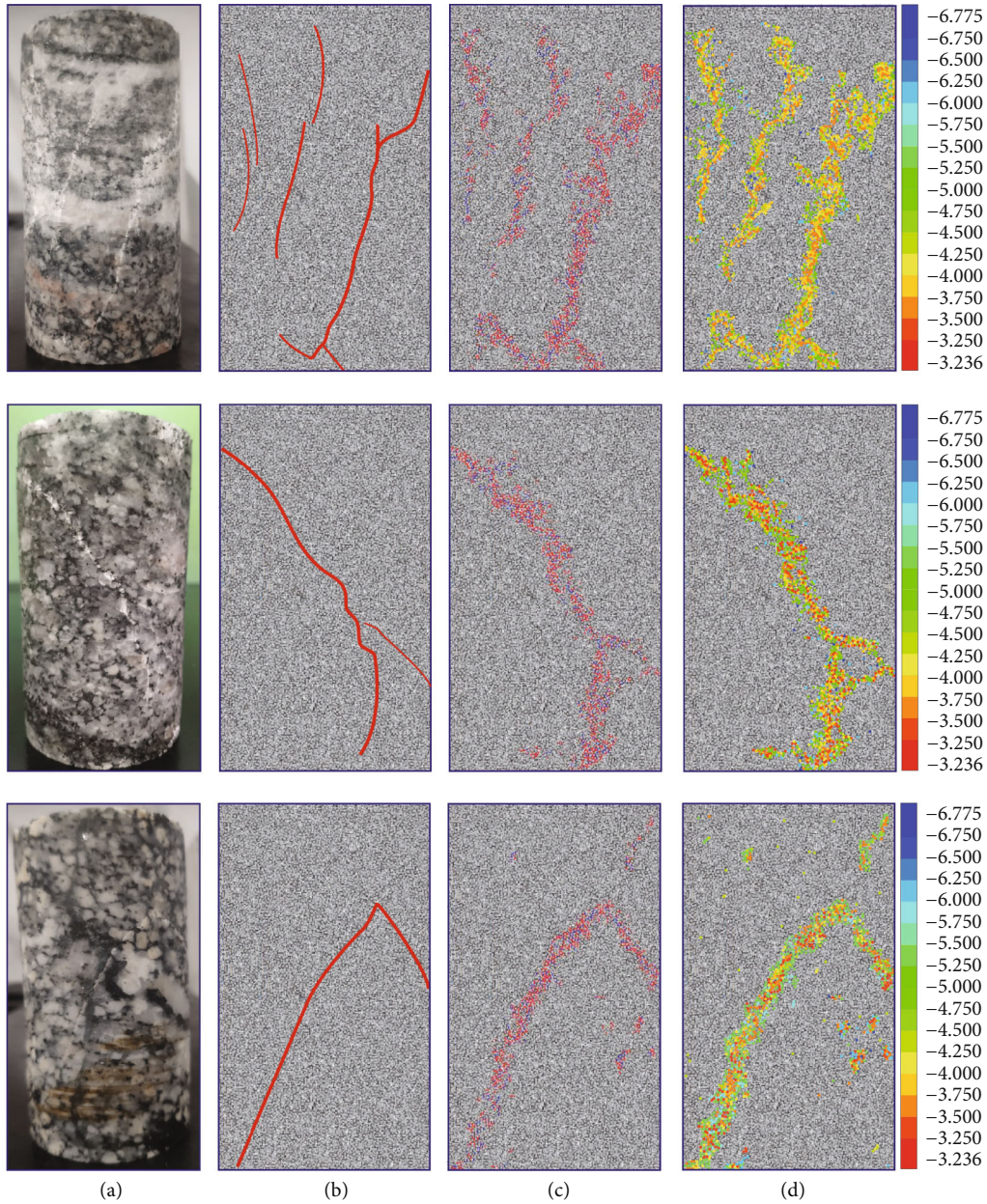

Figure 9: Comparisons of experiment and the simulation results about the fracture morphology: (a) the experimental result; (b) the macroscopic fracture mode of experimental result (schematic diagram); (c) the fracture propagation simulated by the DEM model; (d) the energy released by fracture propagation.

conventional oil and gas reservoirs, there are a large number of natural fractures developed in HDR. Therefore, unlike conventional hydraulic fracturing techniques that use large displacement to form tensile fractures in oil and gas reservoirs, the reactivation of these preexisting fractures through hydraulic shear fracturing techniques is key to the formation of hydraulic fracture networks in HDR [43–45]. Since the granite samples collected in the field for the experiments are mostly homogeneous (without natural fractures), it is difficult to quantitatively study the role of natural fractures in cyclic hydraulic fracturing, resulting in incomplete experimental results [21]. Thus, to further explore new cyclic injection methods, a discrete element fracture network model was constructed by introducing preexisting fractures, and the initiation and propagation of hydraulic fractures under different cyclic injection methods were determined in this work.

3.2.1. The HF Propagation Regime Induced by Low Flow-Low Cycle Interval. Figure 21 shows the HF propagation regime at different approach angles (15°, 30°, 45°, and 60°) using the cyclic injection method with low flow-low cycle interval. When hydraulic fractures encounter natural fractures, the propagation modes of natural fractures can be divided into four categories [46]. For situation where the approach angle is small (15°), hydraulic fracture can fully open the natural

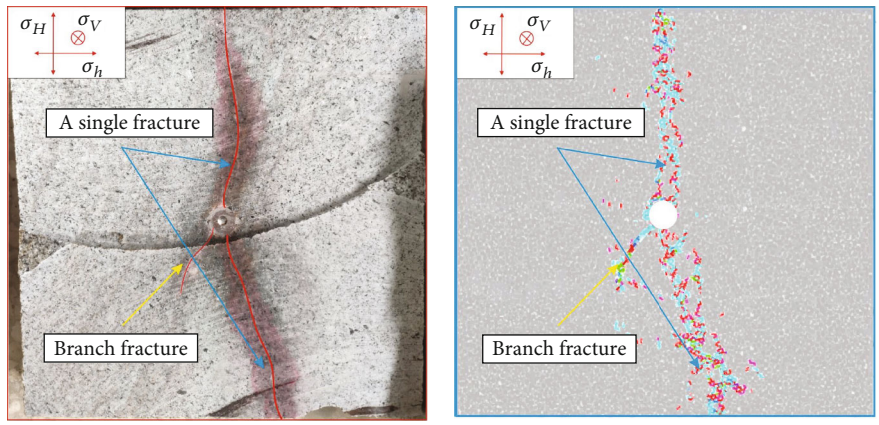

(a) (b)

Figure 10: The hydraulic fracture morphology of the experimental (a) and numerical models (b).

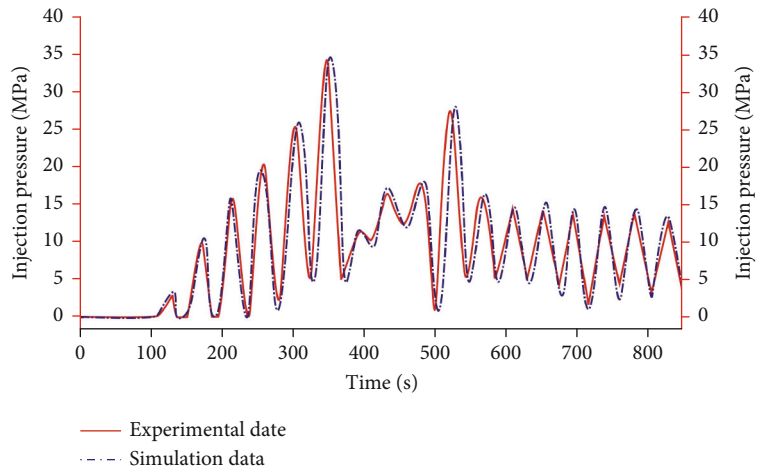

Figure 11: The hydraulic fracturing pressure curve of the numerical and experimental models.

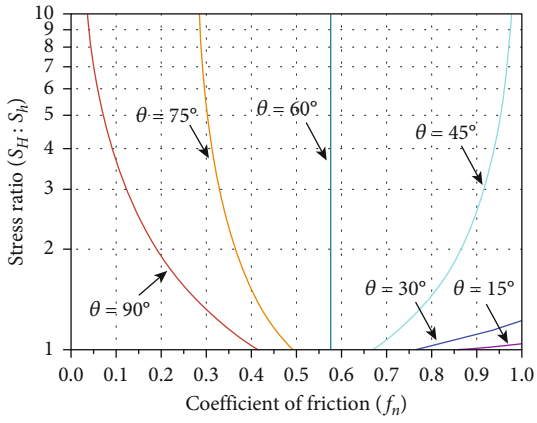

Figure 12: Critical determination curve of HF crossing NFs based on Gu and Weng [38].

fractures, and shear sliding occurs along the natural fractures (type I, Figure 21). With the increase of the approach angle (60°), the propagation mode of hydraulic fracture changes from being captured by natural fractures to directly penetrate through natural fractures and propagating along the original direction (type IV, Figure 21). For the cyclic injection with low flow-low cycle interval, hydraulic fractures can easily capture and propagate along the natural fractures.

The geometry of the stimulated area under the low flow-low cycle interval shows that the propagation of hydraulic fractures is greatly affected by natural fractures, and it is easy to form a nearly circular (planar) hydraulic fracture network. However, due to the small injection displacement, the elliptical fracture network is only limited around the wellbore, and the extension of the fracture network is short (Figure 22).

The reason is that the low flow-low cycle interval cyclic injection is easy to activate natural fractures and create more branched fractures in the rock matrix. However, although the hydraulic fracture network formed by this hydraulic fracturing method is complex, it is difficult to form an effective heat exchange area due to the short propagation range of the fractures.

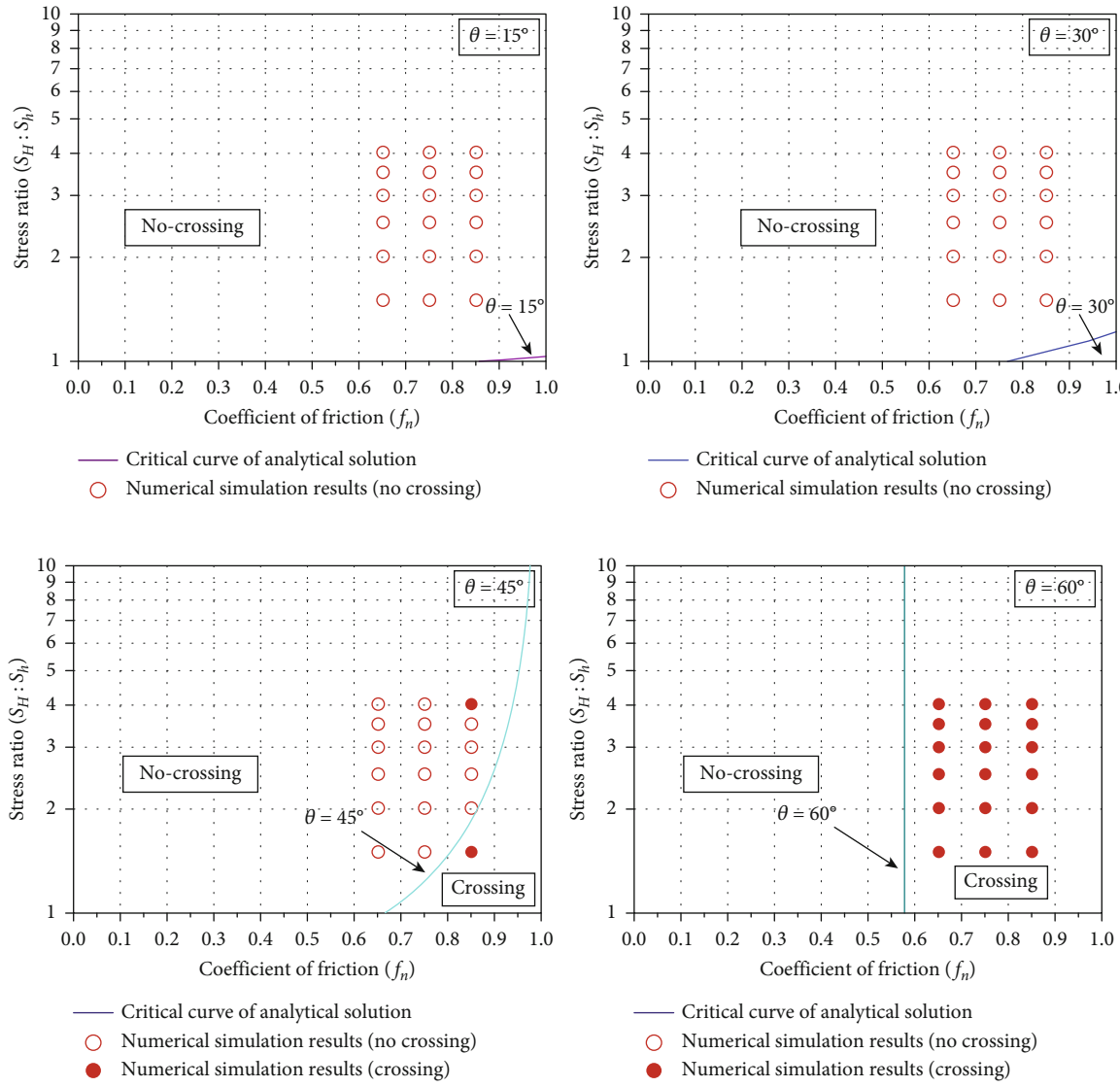

Figure 13: Validation results of numerical simulation and corresponding theoretical analysis.

Table 3: The parameters of natural fractures after calibration.

Parameter	Value	Unit
Normal stiffness	45	N/m^3
Shear stiffness	55	N/m^3
Tensile strength	0.78	MPa
Cohesion	0.64	MPa
Friction angle	22	°
Dilation angle	3	°

3.2.2. The HF Propagation Regime Induced by High Flow-High Cycle Interval. The HF propagation regime induced by high flow-high cycle interval is shown in Figure 23. At a lower intersection angle (15°), the propagation of hydraulic fractures is the same as that of high flow-high cycle interval cyclic injection. When the approach angle gradually increases, it appears to directly penetrate through the natural fractures and continue to propagate along the original direction. Compared with low flow-low cycle interval cyclic injection, high flow-high cycle interval has poor ability to capture natural fractures, and it is easy to produce a simple and straight hydraulic main fracture with fewer branches in the reservoir far from the wellbore (Figure 23).

The geometry of the stimulated area under the high flow-high cycle interval shows that this cyclic injection method has a better stimulation effect around the wellbore due to the high injection pressure. The fractures are distributed in a nearly elliptical shape. However, at the far end of the wellbore, the fracture is mainly along the direction of the MPS, and there is no branch fracture in other directions (Figure 24).

Compared with the low flow-low cycle interval cyclic injection, the high flow-high cycle interval has poorer ability to capture natural fractures, and the hydraulic fractures are easily controlled by in situ stress. Therefore, compared to the low flow-low cycle interval cyclic injection, hydraulic

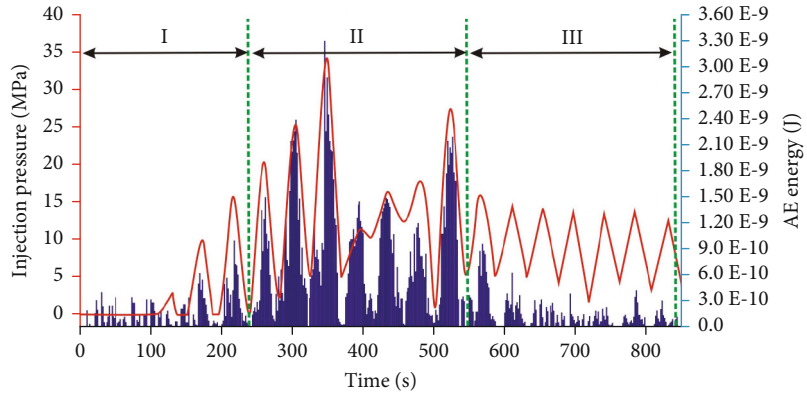

Figure 14: Injection pressure and acoustic emission energy level of high flow-high cycle interval rock sample.

fractures are mainly along the direction of the MPS, and there is no branch fracture in other directions. Additionally, due to the high pressure of this injection method, the main hydraulic fractures formed by the cyclic injection with high flow-high cycle interval have strong extension ability.

3.3. Discussion of Alternating Cyclic Injection Method. Compared to conventional reservoirs, the HDR is subject to high temperature, high stress, and high stress difference conditions. At higher stress differences, the nonuniform allocation of fracturing fluid volume in all directions becomes stronger, and the competitive advantage of hydraulic fractures along the direction of maximum principal stress becomes more obvious. Therefore, it is difficult to form effective branching fractures in other directions [20]. Research suggests that cyclic injection can achieve stress relaxation at the fracture tip through the intermittency of each cycle stage and then generate a new loading state. After the redistribution of the stress, the fluid has the opportunity to find a new flow path in the following injection cycle. This provides the possibility of redistributing fluid flow volume and pressure, regulating the competition between hydraulic fractures, and achieving simultaneous initiation of multiple hydraulic fractures [42, 47].

The results show that the initiation and propagation of fractures are influenced by the injection rate and duration of each cycle. Through the experiments, it can be inferred that when the injection rate and cycle interval are low during the cyclic injection, the range of fluid migration and accumulation in the reservoir is wide, and the uniform pressure increase of the fluid in the reservoir can to some extent regulate the competition relationship between multiple fractures. However, due to the small injection displacement and the dispersed migration of fluids (multiple branch fractures), the injection pressure allocated to each fracture is lower. Currently, the fractures are likely to initiate simultaneously along the circumference of the wellbore, forming complex but relatively short hydraulic fractures.

On the contrary, the increase of injection rate and cycle interval will lead to fluid migration mainly controlled by in situ stress and the nonuniform distribution of fracturing flow volume causing the formation of hydraulic fractures in the reservoir that are simple and straight but have strong expansion ability. Thus, it follows that when the rock material and external conditions are the same, the key parameters of cyclic injection play significant roles in regulating the competition of fractures. The changes in the combination relationship between injection rate and cycle interval induce changes in the competition mechanism, which will inevitably lead to differences in the hydraulic fracture morphology of the reservoir.

Hence, one can see that, at the early stage of fracturing, the low flow-low cycle interval cyclic injection can promote the uniform migration of fluid to the unpressurized area of the reservoir. A uniform increase in fluid pressure can cause natural fractures within the pressurized range to initiate simultaneously. On this basis, the high flow-high cycle interval can promote stable and rapid propagation of the generated fractures by increasing the injection pressure. The alternating fluid injection can fully exploit the merits of the different cyclic injection schemes, thus forming a large volume fracturing network.

3.4. Fracture Network Simulation of HDR under the Alternating Cyclic Injection Method. The different cyclic injection methods play different roles in the development of the HDR hydraulic fracturing. To fully improve the complexity of the hydraulic fracture network and consider the hydraulic stimulation area, an alternating cyclic injection method with synergistic control of the cyclic frequency and injection rate is proposed in this work. The total injection amount of the alternating cyclic injection method (i.e., combined the low flow-low cycle interval and the high flow-high cycle interval injection scheme) is consistent with the single low flow-low cycle interval and high flow-high cycle interval injection method (e.g., 360 m^2).

Compared with the single injection methods (low flow-low cycle interval and high flow-high cycle interval) (Figures 25(b) and 25(c)), the alternating cyclic injection method produced a larger stimulation area (Figure 25(a)). When the total injection volume of all injection methods is 360 m^2, the stimulation area of the alternating cyclic injection method (stimulation area = 9.8×10^3 m^2) is about 2.3 times and 2.7 times that of the low flow-low frequency (stimulation area = 4.2×10^3 m^2) and the high flow-high frequency (stimulation area = 3.6×10^3 m^2) (Figure 26). In

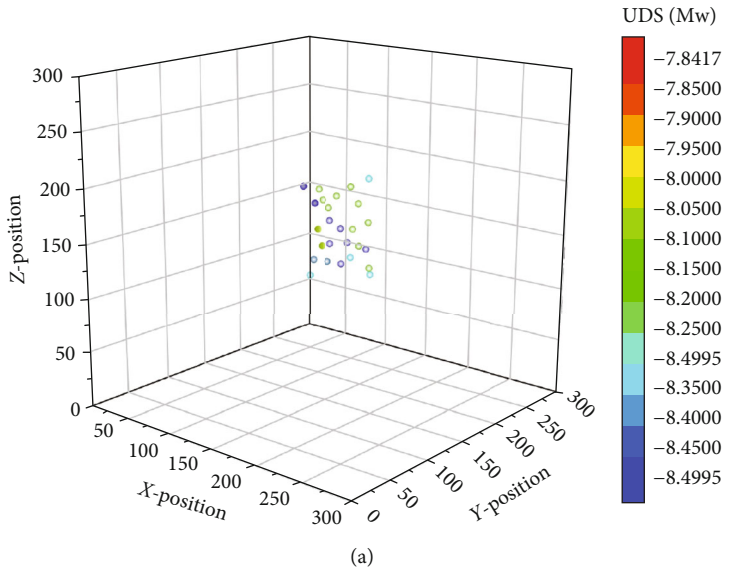

(a)

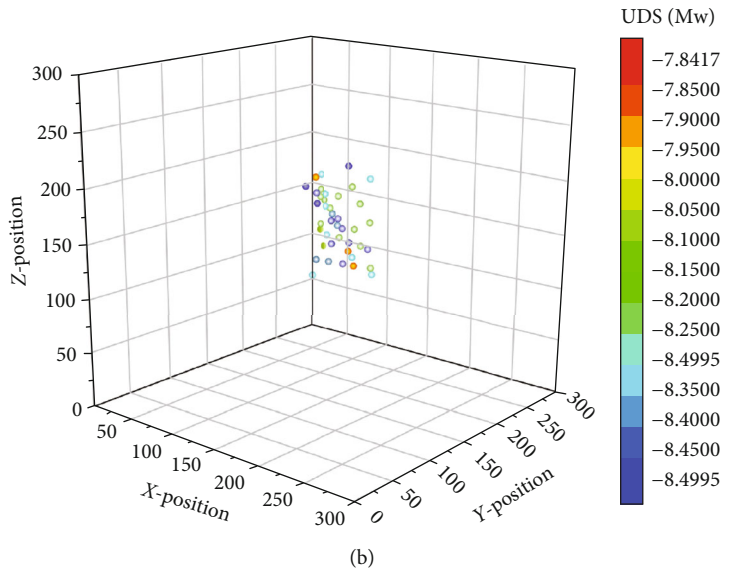

(b)

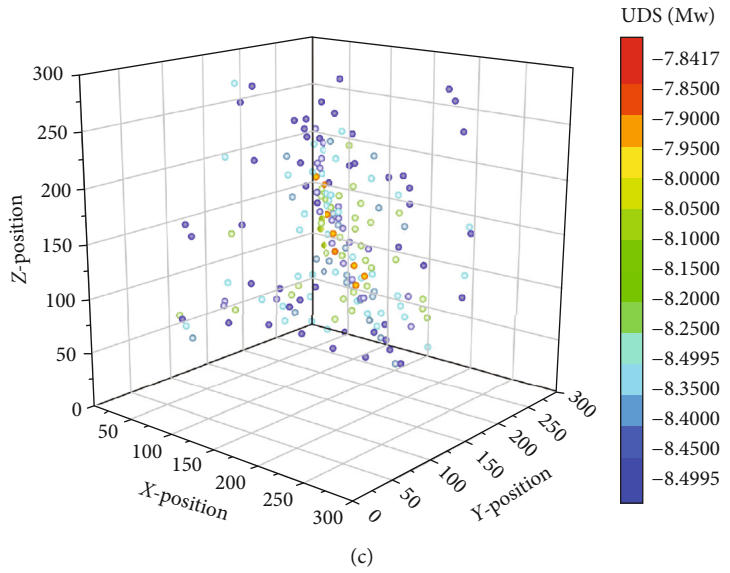

(c)

Figure 15: Continued.

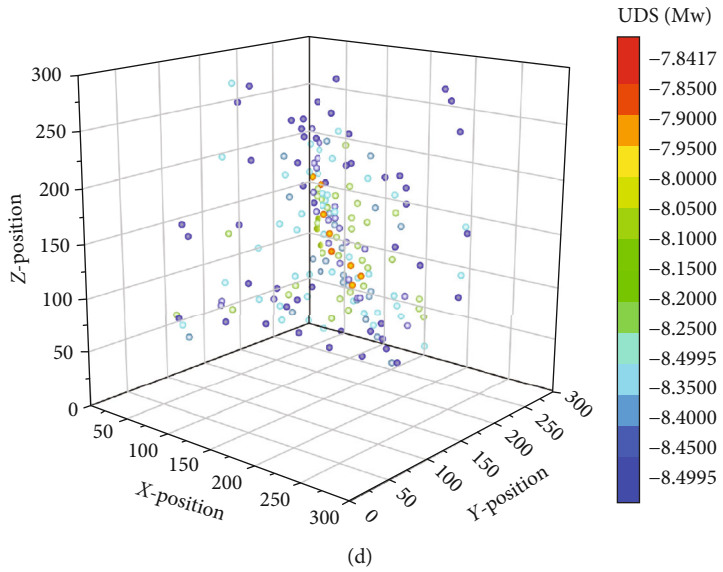

Figure 15: The spatial distribution of acoustic emission points under the cyclic injection with high flow-high frequency.

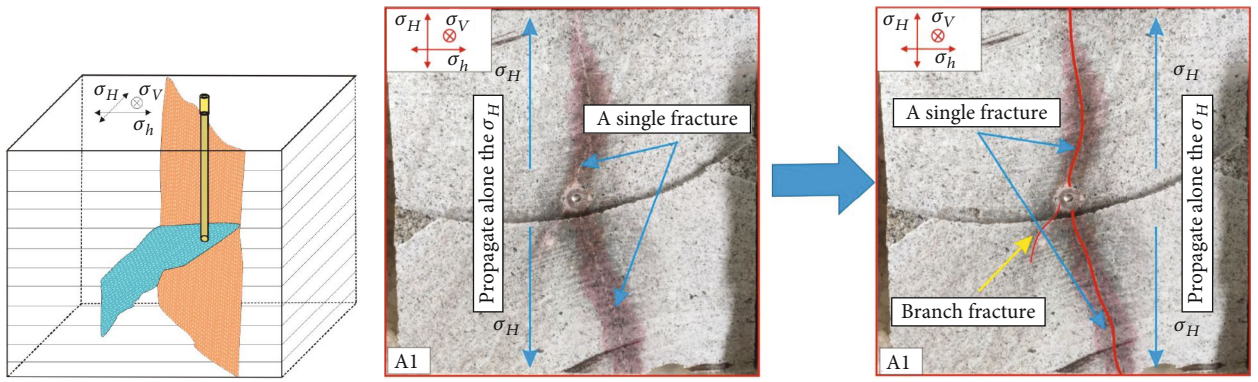

Figure 16: Hydraulic fracture geometry of high flow-high cycle interval rock sample after hydraulic fracturing.

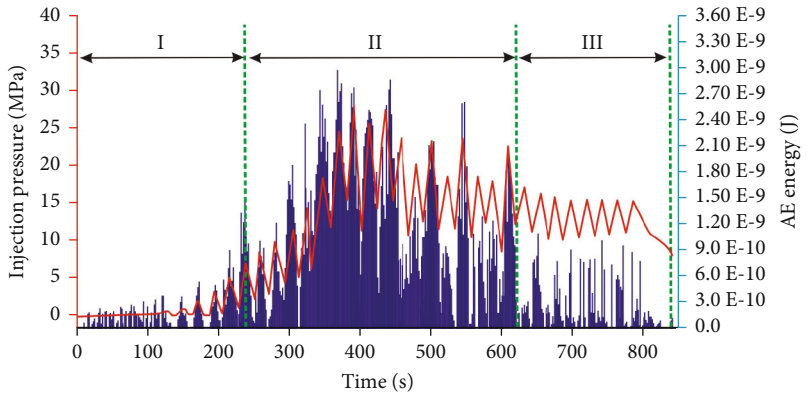

Figure 17: Injection pressure and acoustic emission energy level of low flow-low cycle interval rock sample.

addition, the average aperture of hydraulic fractures of the alternating cyclic injection method is acceptable compared to the low flow-low cycle interval and high flow-high cycle interval injection methods. The results indicated that the proposed alternating cyclic injection method can effectively improve the fracturing effect of the HDR.

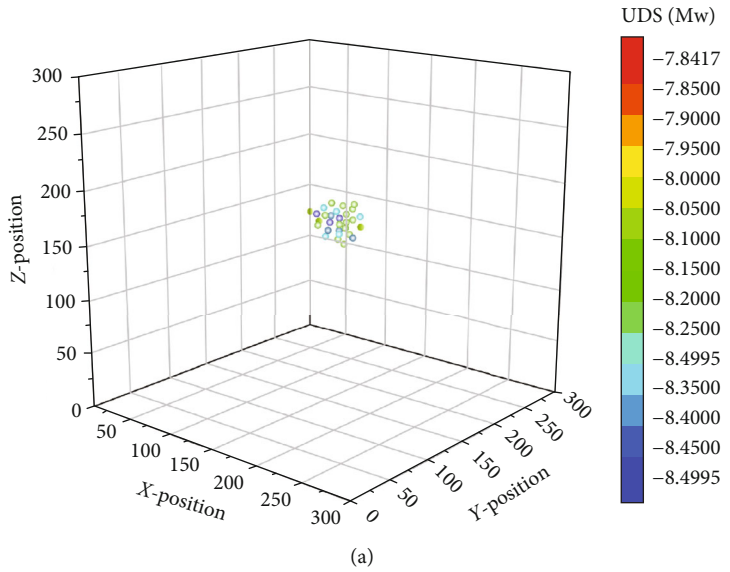

(a)

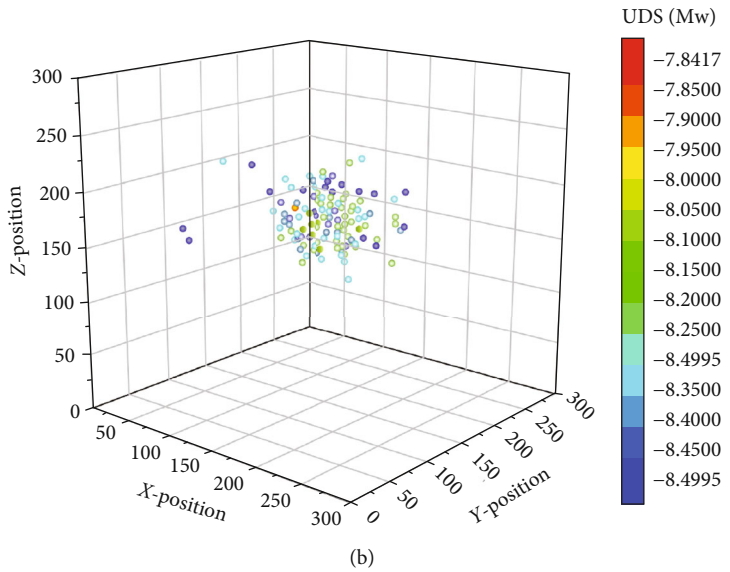

(b)

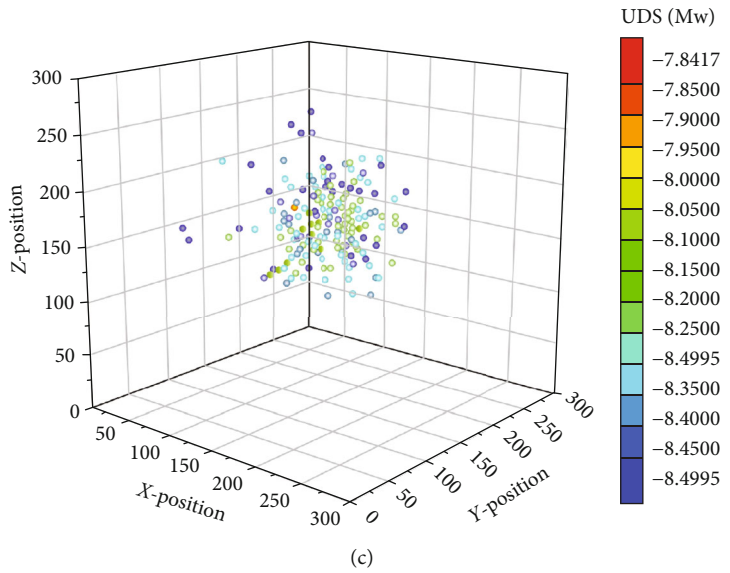

(c)

Figure 18: Continued.

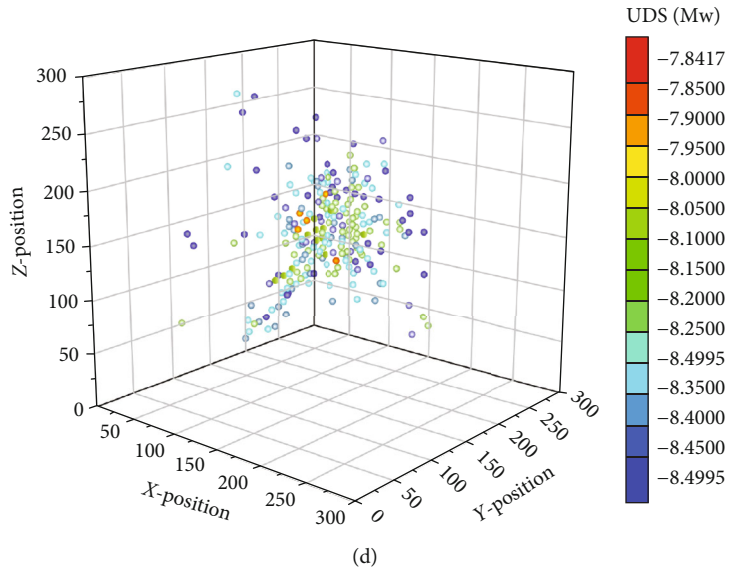

Figure 18: The spatial distribution of acoustic emission points under the cyclic injection with low flow-low cycle interval.

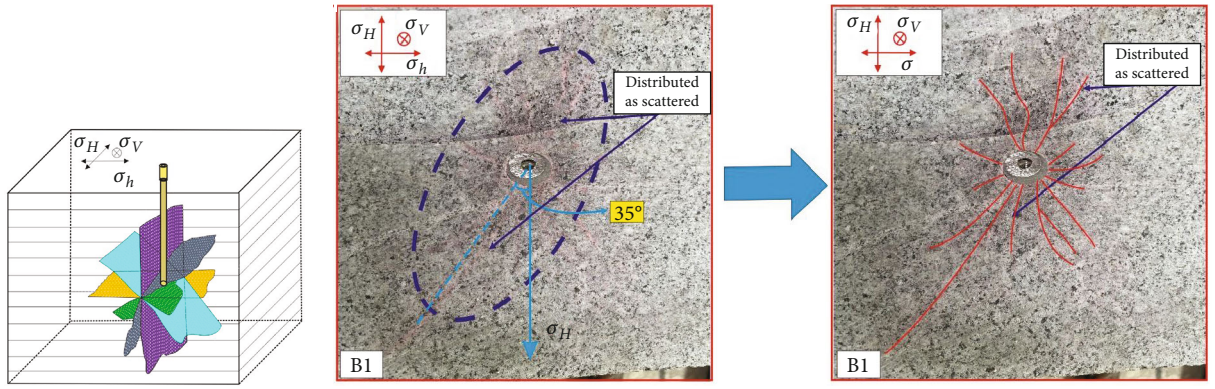

Figure 19: Hydraulic fracture geometry of low flow-low cycle interval rock sample after hydraulic fracturing.

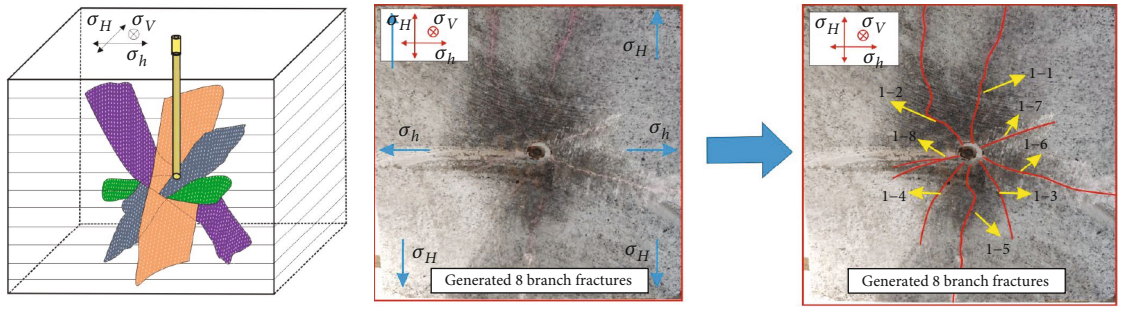

Figure 20: Hydraulic fracture geometry of alternating cyclic injection.

4. Conclusions

True triaxial hydraulic fracturing platform was adapted to systematically study the initiation and propagation of hydraulic fractures in the HDR under different cyclic injection methods. On this basis, by constructing a discrete fracture network model, the initiation and propagation of hydraulic fractures under single and alternating injection methods were

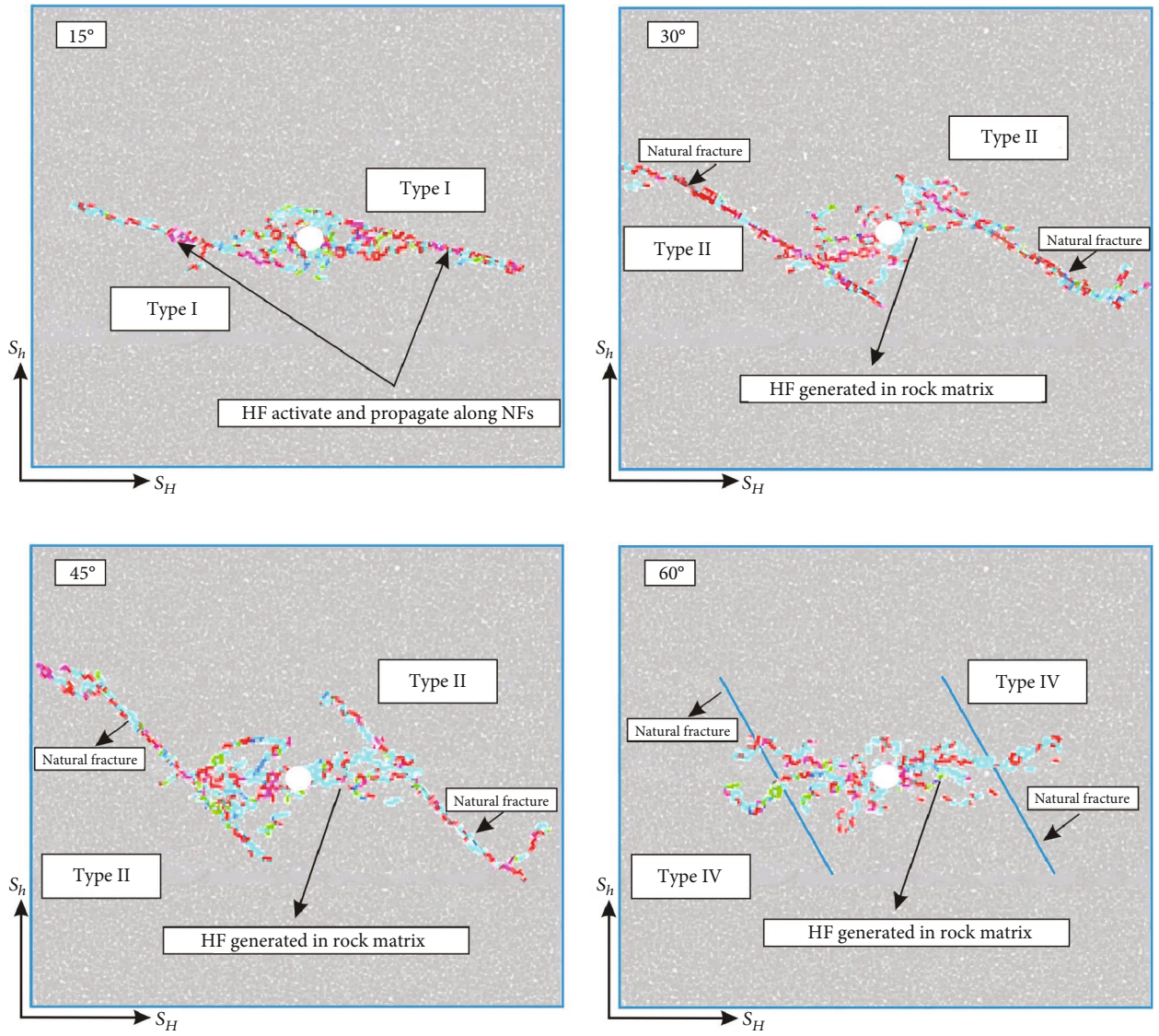

Figure 21: Mechanism of HF propagation under low flow-low cycle interval cyclic injection method.

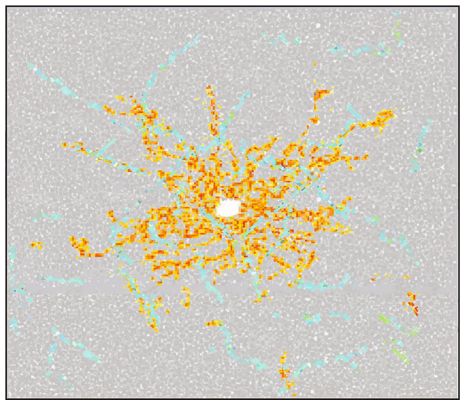

Figure 22: The geometry of the stimulated area under the low flow-low cycle interval cyclic injection method.

determined. As a result, an alternating cyclic injection scheme with synergistic control of the cyclic frequency and injection rate was proposed for improving the hydraulic fracturing effect. Based on experimental and numerical model studies, the following conclusions are drawn:

(1) The impact of cyclic injection methods on hydraulic fracture propagation regimes was determined by experiment research for hydraulic fracturing. The results show that different cyclic injection methods played different roles in the stimulation of HDR. High flow-high cycle interval cyclic injection can easily form fractures with single morphology but strong extensibility, while the fractures formed by low flow-low cycle interval cyclic injection are complex but have a short extension range

(2) Different cyclic injection methods can lead to different propagation regimes and ultimately result in

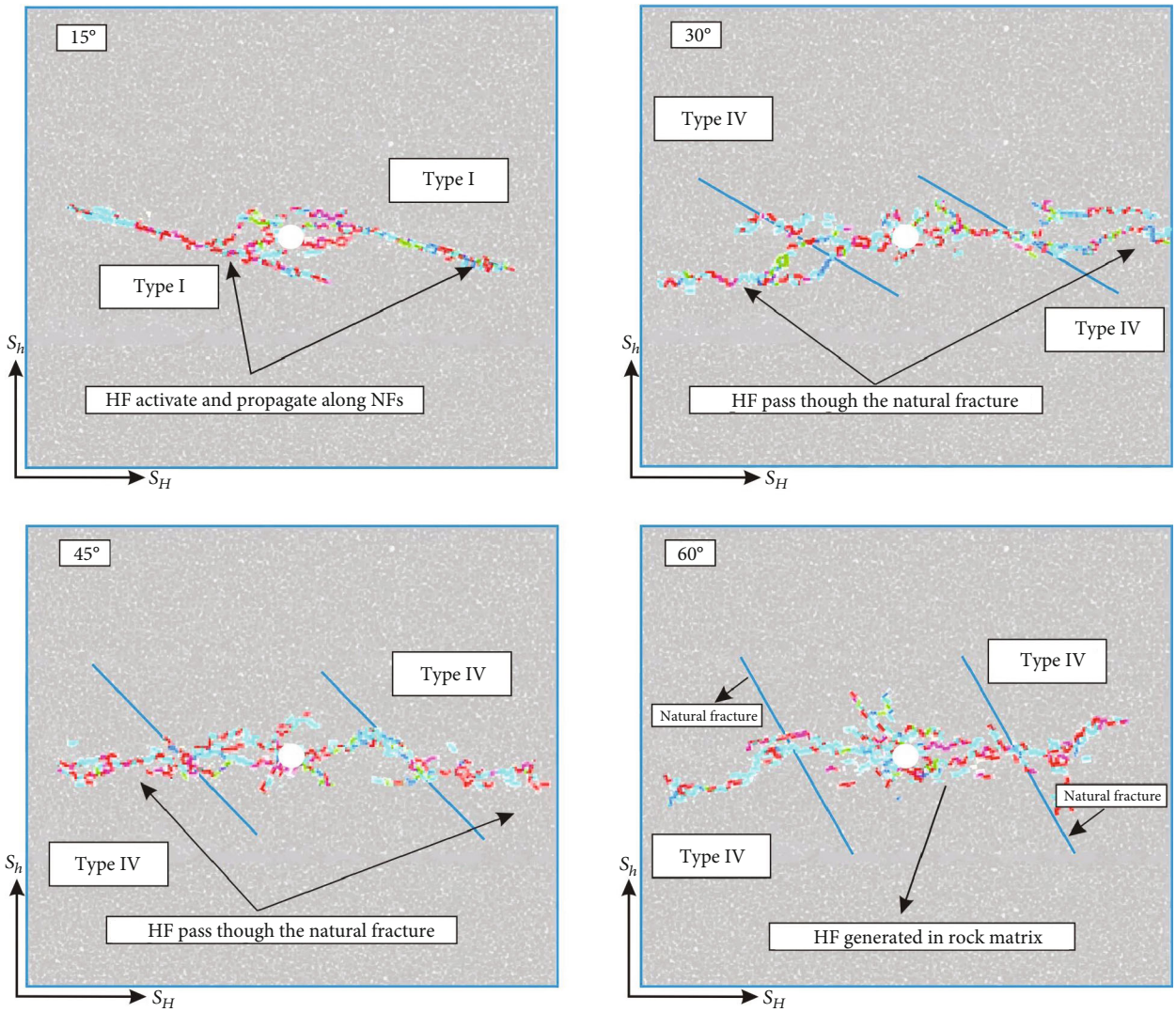

Figure 23: Mechanism of HF propagation under high flow-high cycle interval cyclic injection method.

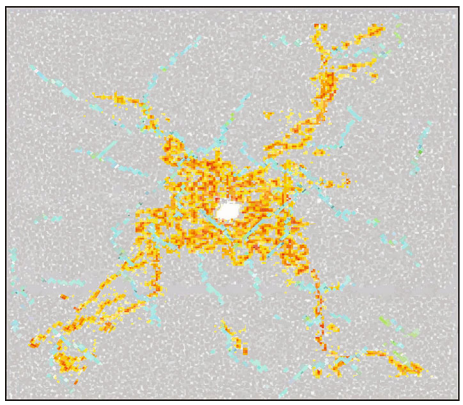

Figure 24: The geometry of the stimulated area under the high flow-high cycle interval cyclic injection method.

variation of the fracture network. Thus, a numerical model that contains a fracture network was established with PFC2D software, and the impact of cyclic injection methods on the hydraulic fracture network formation was investigated systematically. The results show that the expansion of hydraulic fractures is greatly affected by natural fractures, and it is easy to form a complex but short hydraulic fracture network under the low flow-low cycle interval cyclic injection, while the hydraulic fractures under the high flow-high cycle interval generally extend asymmetrically along the MPS and tend to form a narrow and long strip-shaped hydraulic fracture network

(3) Different cyclic injection methods play different roles in the formation of hydraulic fractures, and each has its own merits and disadvantages. To fully exploit the advantages of the different cyclic injection schemes, an alternating cyclic injection scheme with synergistic control of the cyclic cycle interval and injection rate was proposed. The results show that the alternating cyclic injection scheme can fully exploit the merits of the different cyclic injection

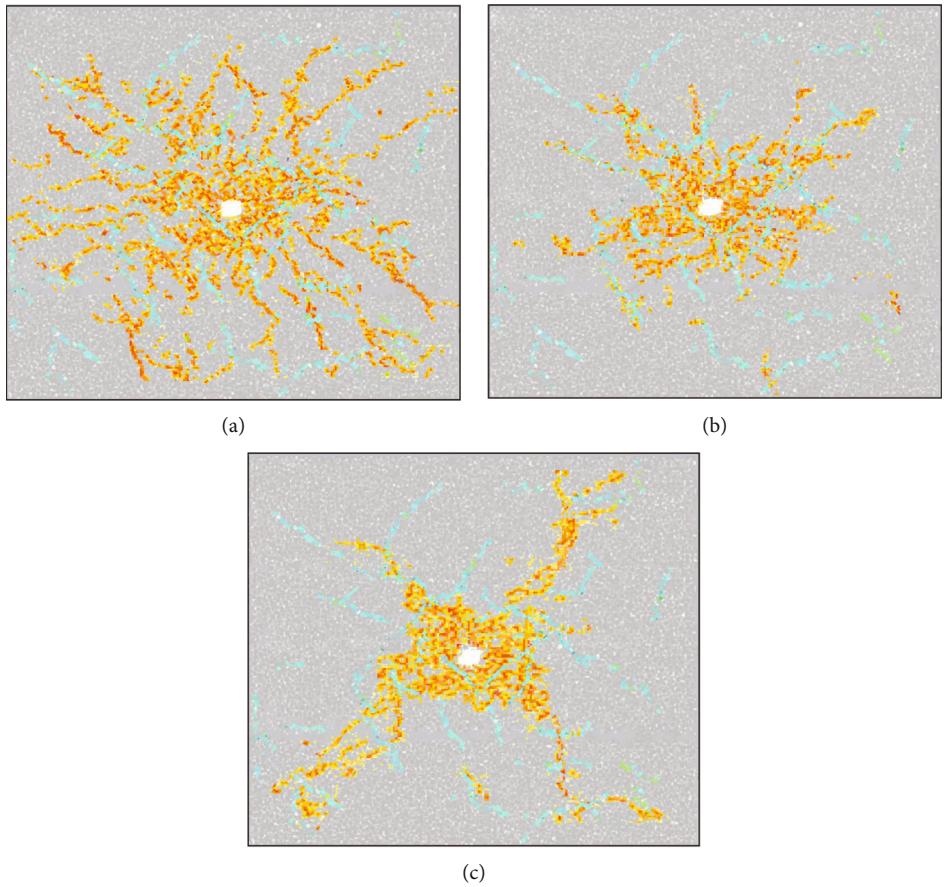

Figure 25: The fracturing effects between single and the alternating cyclic injection method: (a) alternating cyclic injection method, (b) low flow-low cycle interval, and (c) high flow-high cycle interval.

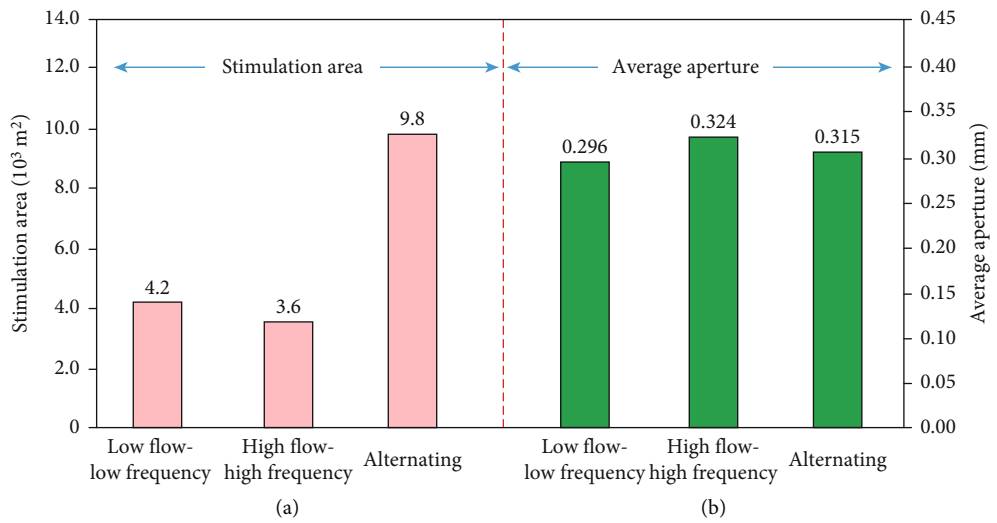

Figure 26: The stimulation area (a) and average aperture (b) for the low flow-low cycle interval, high flow-high cycle interval, and alternating cyclic injection method.

schemes and may also offer some advantages, and the fracturing area of the alternating cyclic injection method is 2.3~2.7 times that of the single injection schemes. The method presented here can be adopted to optimize the fracture growth regime and provide a scientific basis for EGS hydraulic fracturing design

Data Availability

All relevant data are within the manuscript.

Conflicts of Interest

No conflict of interest exits in the submission of this manuscript.

Authors' Contributions

The manuscript is approved by all authors for publication.

Acknowledgments

This work is jointly supported by the Open Fund of State Key Laboratory of Water Resource Protection and Utilization in Coal Mining (Grant No. GJNY-21-41-13) and Jilin Province Science and Technology Development Plan Project (Grant No. 20220101160JC).

References

[1] Z. Hu, T. F. Xu, J. Moore et al., "Investigation of the effect of different injection schemes on fracture network patterns in hot dry rocks - a numerical case study of the FORGE EGS site in Utah," *Journal of Natural Gas Science and Engineering*, vol. 97, article 104346, 2022.

[2] D. J. Tomas, "Abandoned coal mine geothermal for future wide scale heat networks," *Fuel*, vol. 189, p. 445, 2017.

[3] M. O. Haring, U. Schanz, F. Ladner, and B. C. Dyer, "Characterisation of the Basel 1 enhanced geothermal system," *Geothermics*, vol. 37, no. 5, pp. 469–495, 2008.

[4] H. Hofmann, T. Babadagli, and G. Zimmermann, "Hot water generation for oil sands processing from enhanced geothermal systems: process simulation for different hydraulic fracturing scenarios," *Applied Energy*, vol. 113, pp. 524–547, 2014.

[5] C. Dezayes, A. Genter, and B. Valley, "Structure du reseau de fractures naturelles dans le reservoir geothermique peu permeable de Soultz," *Comptes Rendus Geoscience*, vol. 342, no. 7-8, pp. 517–530, 2010.

[6] J. Riffault, D. Dempsey, S. Karra, and R. Archer, "Microseismicity cloud can be substantially larger than the associated stimulated fracture volume: the case of the Paralana enhanced geothermal system," *Journal of Geophysical Research - Solid Earth*, vol. 123, no. 8, pp. 6845–6870, 2018.

[7] Y. Xue, J. Liu, X. Liang et al., "Influence mechanism of brine-gas two-phase flow on sealing property of anisotropic caprock for hydrogen and carbon energy underground storage," *International Journal of Hydrogen Energy*, vol. 48, no. 30, pp. 11287–11302, 2023.

[8] B. S. Wu, X. Zhang, R. G. Jeffrey, A. P. Bunger, and S. Jia, "A simplified model for heat extraction by circulating fluid through a closed- loop multiple-fracture enhanced geothermal system," *Applied Energy*, vol. 183, pp. 1664–1681, 2016.

[9] Y. Liu, T. F. Xu, Y. L. Yuan et al., "Discrete element modeling for the multistage hydraulic stimulation of a horizontal well in hot dry rock," *Computers and Geotechnics*, vol. 156, article 105274, 2023.

[10] Y. Xue, S. Liu, J. Chai et al., "Effect of water-cooling shock on fracture initiation and morphology of high- temperature granite: application of hydraulic fracturing to enhanced geothermal systems," *Applied Energy*, vol. 337, p. 120858, 2023.

[11] P. L. Yu, D. Dempsey, and R. Archer, "A three-dimensional coupled thermo-hydro-mechanical numerical model with partially bridging multi-stage contact fractures in horizontal-well enhanced geothermal system," *International Journal of Rock Mechanics and Mining Sciences*, vol. 143, article 104787, 2021.

[12] A. Dahi-Taleghani, M. Gonzalez, and A. Shojaei, "Overview of numerical models for interactions between hydraulic fractures and natural fractures: challenges and limitations," *Computers and Geotechnics*, vol. 71, pp. 361–369, 2016.

[13] M. B. Diaz, K. Y. Kim, and S. G. Jung, "Effect of frequency during cyclic hydraulic fracturing and the process of fracture development in laboratory experiments," *International Journal of Rock Mechanics and Mining Sciences*, vol. 134, p. 104474, 2020.

[14] A. Zang, G. Zimmermann, H. Hofmann, O. Stephansson, K. B. Min, and K. Y. Kim, "How to reduce fluid-injection-induced seismicity," *Rock Mechanics and Rock Engineering*, vol. 52, no. 2, pp. 475–493, 2019.

[15] Z. Li, S. G. Jung, M. Diaz, K. Y. Kim, and J. S. Yoon, "Laboratory true triaxial hydraulic fracturing of granite under six fluid injection schemes and grain-scale fracture observations," *Rock Mechanics and Rock Engineering*, vol. 53, no. 10, pp. 4329–4344, 2020.

[16] A. Zang, J. S. Yoon, O. Stephansson, and O. Heidbach, "Fatigue hydraulic fracturing by cyclic reservoir treatment enhances permeability and reduces induced seismicity," *Geophysical Journal International*, vol. 195, no. 2, pp. 1282–1287, 2013.

[17] I. Zimmermann and G. Moeck, "Cyclic waterfrac stimulation to develop an enhanced geothermal system (EGS)–conceptual design and experimental results," *Geothermics*, vol. 39, no. 1, pp. 59–69, 2010.

[18] A. Zang, F. C. Wagner, S. Stanchits, C. Janssen, and G. Dresen, "Fracture process zone in granite," *Journal of Geophysical Research*, vol. 105, no. B10, pp. 23651–23661, 2000.

[19] M. N. Bagde and V. Petroš, "The effect of micro-structure on fatigue behaviour of intact sandstone," *International Journal of Geo-Information*, vol. 2, no. 3, pp. 240–247, 2011.

[20] N. Erarslan and D. J. Williams, "Investigating the effect of cyclic loading on the indirect tensile strength of rocks," *Rock Mechanics and Rock Engineering*, vol. 45, no. 3, pp. 327–340, 2012.

[21] Z. Li, Y. K. Wang, and G. J. Sung, "Cyclic hydraulic fracturing of Pocheon granite cores and its impact on breakdown pressure, acoustic emission amplitudes and injectivity," *International Journal of Rock Mechanics and Mining Sciences*, vol. 122, article 104065, 2019.

[22] Y. Hou, Y. Peng, Z. Chen et al., "Investigation on the controlling factors of pressure wave propagation behavior induced by pulsating hydraulic fracturing," *SPE Journal*, vol. 26, no. 5, pp. 2716–2735, 2021.

[23] Z. L. Zhou, G. Q. Zhang, Y. K. Xing, Z. Y. Fan, X. Zhang, and D. Kasperczyk, "A laboratory study of multiple fracture initiation from perforation clusters by cyclic pumping," *Rock Mechanics and Rock Engineering*, vol. 52, no. 3, pp. 827–840, 2019.

[24] N. Erarslan and D. J. Williams, "Mixed-mode fracturing of rocks under static and cyclic loading," *Rock Mechanics and Rock Engineering*, vol. 46, no. 5, pp. 1035–1052, 2013.

[25] C. Sun, H. Zheng, W. D. Liu, and W. Lu, "Numerical investigation of complex fracture network creation by cyclic pumping," *Engineering Fracture Mechanics*, vol. 233, article 107103, 2020.

[26] J. S. Yoon, G. Zimmermann, and A. Zang, "Discrete element modeling of cyclic rate fluid injection at multiple locations in naturally fractured reservoirs," *International Journal of Rock Mechanics and Mining Sciences*, vol. 74, pp. 15–23, 2015.

[27] A. Zang, O. Stephansson, and G. Zimmermann, "Keynote: fatigue hydraulic fracturing," *Procedia Engineering*, vol. 191, pp. 1126–1134, 2017.

[28] L. Zhuang, K. Y. Kim, and S. G. Jung, "Laboratory investigation of hydraulic fracturing of granite under true triaxial stress state using different injection schemes-part 1. Permeability enhancement," in *International Conference on Coupled Processes in Fractured Geological Media: Observation, Modeling, and Application*, Wuhan, 2018.

[29] D. Chuprakov, O. Melchaeva, and R. Prioul, "Injection-sensitive mechanics of hydraulic fracture interaction with discontinuities," *Rock Mechanics and Rock Engineering*, vol. 47, no. 5, pp. 1625–1640, 2014.

[30] M. Sheng, P. Li, X. Zhuang, and J. Wang, "Influence of cyclic normal stress on shear friction of EGS granite fractures," *Engineering Fracture Mechanics*, vol. 238, p. 107268, 2020.

[31] Y. Liu, T. F. Xu, Y. L. Yuan et al., "A laboratory study on fracture initiation and propagation of granite under cyclic-injection hydraulic fracturing," *Journal of Petroleum Science and Engineering*, vol. 212, article 110278, 2022.

[32] L. Xie, K. B. Min, and Y. Song, "Observations of hydraulic stimulations in seven enhanced geothermal system projects," *Renewable Energy*, vol. 79, pp. 56–65, 2015.

[33] D. O. Potyondy and P. A. Cundall, "A bonded-particle model for rock," *International Journal of Rock Mechanics and Mining Sciences*, vol. 41, no. 8, pp. 1329–1364, 2004.

[34] Itasca Consulting Group Inc, *Users' Manual for Particle Flow Code (PFC), Version 5.0 Minneapolis, Minnesota*, Itasca Consulting Group Inc, 2014.

[35] Z. Chong, S. Karekal, X. Li, P. Hou, G. Yang, and S. Liang, "Numerical investigation of hydraulic fracturing in transversely isotropic shale reservoirs based on the discrete element method," *Journal of Natural Gas Science and Engineering*, vol. 46, pp. 398–420, 2017.

[36] S. Nadimi, B. Forbes, J. Moore, and J. McLennan, "Effect of natural fractures on determining closure pressure," *Journal of Petroleum Exploration and Production Technology*, vol. 10, pp. 711–728, 2020.

[37] S. Nadimi, B. Forbes, J. Moore, R. Podgorney, and J. D. Mclennan, "Utah FORGE: hydrogeothermal modeling of a granitic based discrete fracture network," *Geothermics*, vol. 87, p. 101853, 2020.

[38] H. Gu and X. Weng, "Criterion for fractures crossing frictional interfaces at non-orthogonal angles," in *44th US Rock Mechanics Symposium and 5th US-Canada Rock Mechanics symposium American Rock Mechanics Association*, ARMA, 2010.

[39] L. Tong, W. Xiaochen, L. Xiangjun et al., "A criterion for a hydraulic fracture crossing a natural fracture in toughness dominant regime and viscosity dominant regime," *Engineering Fracture Mechanics*, vol. 289, article 109421, 2023.

[40] C. E. Renshaw and D. D. Pollard, "An experimentally verified criterion for propagation across unbounded frictional interfaces in brittle, linear elastic materials," *Pergamon*, vol. 32, no. 3, pp. 237–249, 1995.

[41] Z. J. Zhao, D. A. Liu, Z. D. Cui, and T. T. W. Han, "Cyclic progressive pressure on the fracturing effect of shale," *Chinese Journal of Rock Mechanics and Engineering*, vol. 38, pp. 2779–2789, 2019.

[42] F. Stank, L. Eisner, and T. J. Moser, "Stability of source mechanisms inverted from P-wave amplitude microseismic monitoring data acquired at the surface," *Geophysical Prospecting*, vol. 62, no. 3, pp. 475–490, 2014.

[43] H. Gu, X. Weng, J. B. Lund, M. G. Mack, U. Ganguly, and R. Suarez-Rivera, "Hydraulic fracture crossing natural fracture at nonorthogonal angles: a criterion and its validation," *SPE Production & Operations*, vol. 27, no. 1, pp. 20–26, 2012.

[44] A. Riahi, W. Pettitt, B. Damjanac, and B. Varun, "Numerical modeling of discrete fractures in a field-scale Forge EGS reservoir," *Rock Mechanics and Rock Engineering*, vol. 52, no. 12, pp. 5245–5258, 2019.

[45] T. Wang, W. R. Hu, and E. Derek, "The effect of natural fractures on hydraulic fracturing propagation in coal seams," *Journal of Petroleum Science and Engineering*, vol. 150, pp. 180–190, 2017.

[46] Z. Chong, Q. Yao, X. Li, and J. Liu, "Investigations of seismicity induced by hydraulic fracturing in naturally fractured reservoirs based on moment tensors," *Journal of Natural Gas Science and Engineering*, vol. 81, p. 103448, 2020.

[47] S. Tong and D. Gao, "Basic research progress and development suggestions on hydraulic fracturing," *Oil Drilling Production Tech*, vol. 41, pp. 101–115, 2019.